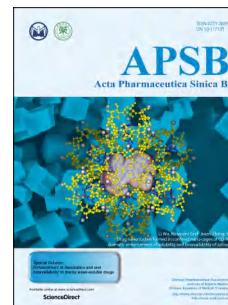


Journal Pre-proof

Targeting Kindlin-2 in adipocytes increases bone mass through inhibiting FAS/PPAR γ /FABP4 signaling in mice

Wanze Tang, Zhen Ding, Huanqing Gao, Qinnan Yan, Jingping Liu, Yingying Han, Xiaoting Hou, Zhengwei Liu, Litong Chen, Dazhi Yang, Guixing Ma, Huiling Cao



PII: S2211-3835(23)00251-4

DOI: <https://doi.org/10.1016/j.apsb.2023.07.001>

Reference: APSB 1731

To appear in: *Acta Pharmaceutica Sinica B*

Received Date: 24 February 2023

Revised Date: 14 May 2023

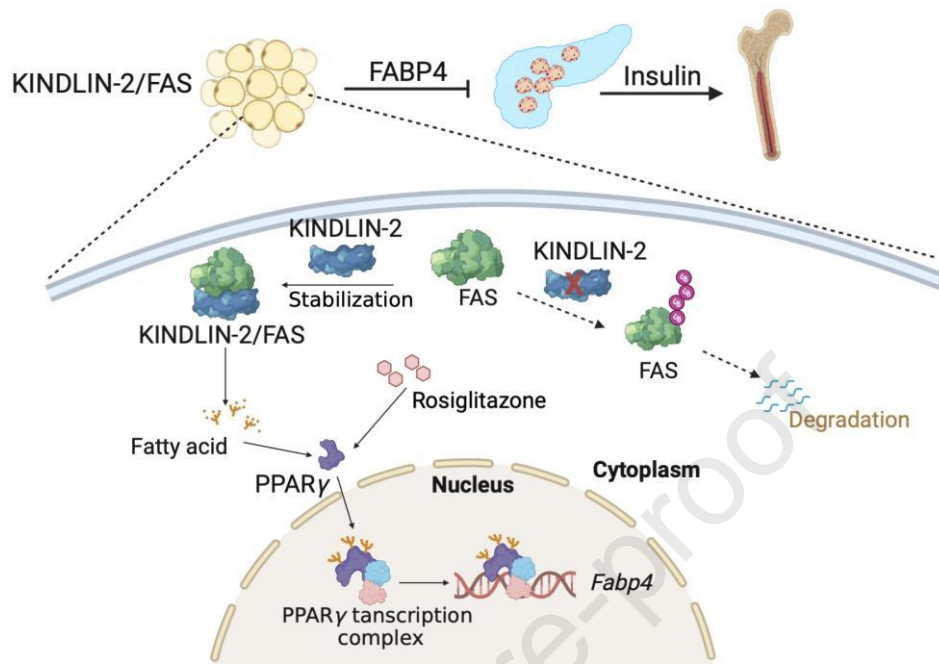
Accepted Date: 18 May 2023

Please cite this article as: Tang W, Ding Z, Gao H, Yan Q, Liu J, Han Y, Hou X, Liu Z, Chen L, Yang D, Ma G, Cao H, Targeting Kindlin-2 in adipocytes increases bone mass through inhibiting FAS/PPAR γ /FABP4 signaling in mice, *Acta Pharmaceutica Sinica B*, <https://doi.org/10.1016/j.apsb.2023.07.001>.

This is a PDF file of an article that has undergone enhancements after acceptance, such as the addition of a cover page and metadata, and formatting for readability, but it is not yet the definitive version of record. This version will undergo additional copyediting, typesetting and review before it is published in its final form, but we are providing this version to give early visibility of the article. Please note that, during the production process, errors may be discovered which could affect the content, and all legal disclaimers that apply to the journal pertain.

© 2023 Chinese Pharmaceutical Association and Institute of Materia Medica, Chinese Academy of Medical Sciences. Production and hosting by Elsevier B.V. All rights reserved.

Graphical abstract



Adipocytes Kindlin-2 enhances Fas stability, which promotes PPAR γ /Fabp4 signaling, leading to reduced insulin level and bone mass. Adipocytes Kindlin-2 and Fas are potential targets for osteoporosis treatment.

Original article

Targeting Kindlin-2 in adipocytes increases bone mass through inhibiting FAS/PPAR γ /FABP4 signaling in mice

Wanze Tang^{a,b,†}, Zhen Ding^{a,†}, Huanqing Gao^{a,†}, Qinnan Yan^{a,†}, Jingping Liu^c, Yingying Han^a, Xiaoting Hou^a, Zhengwei Liu^a, Litong Chen^a, Dazhi Yang^{b,*}, Guixing Ma^{a,*}, Huiling Cao^{a,*}

^aDepartment of Biochemistry, School of Medicine, Southern University of Science and Technology, Guangdong Provincial Key Laboratory of Cell Microenvironment and Disease Research, Key University Laboratory of Metabolism and Health of Guangdong, Southern University of Science and Technology, Shenzhen 518055, China

^bThe First Affiliated Hospital, Southern University of Science and Technology, Shenzhen 518055, China

^cClinical Laboratory of the Third Affiliated Hospital of Southern Medical University, Guangzhou 510630, China

Received 24 February 2023; received in revised form 14 May 2023; accepted 18 May 2023

*Corresponding authors.

E-mail addresses: caohl@sustech.edu.cn (Huiling Cao); magx@mail.sustech.edu.cn (Guixing Ma); yangdazhi1111@163.com (Dazhi Yang).

[†]These authors made equal contributions to this work.

Running title: Kindlin-2 inhibition in adipocytes increases systemic bone mass

Abstract Osteoporosis (OP) is a systemic skeletal disease that primarily affects the elderly population, which greatly increases the risk of fractures. Here we report that Kindlin-2 expression in adipose tissue increases during aging and high-fat diet fed and is accompanied by decreased bone mass. Kindlin-2 specific deletion (K2KO) controlled by *Adipoq-Cre* mice or adipose tissue-targeting AAV (AAV-Rec2-CasRx-sgK2) significantly increases bone mass. Mechanistically, Kindlin-2 promotes peroxisome proliferator-activated receptor gamma (PPAR γ) activation and downstream fatty acid binding protein 4 (FABP4) expression through stabilizing fatty acid synthase (FAS), and increased FABP4 inhibits insulin expression and decreases bone mass. Kindlin-2 inhibition results in accelerated FAS degradation, decreased PPAR γ activation and FABP4 expression, and therefore increased insulin expression and bone mass. Interestingly, we find that FABP4 is increased while insulin is decreased in serum of

OP patients. Increased FABP4 expression through PPAR γ activation by rosiglitazone reverses the high bone mass phenotype of K2KO mice. Inhibition of FAS by C75 phenocopies the high bone mass phenotype of K2KO mice. Collectively, our study establishes a novel Kindlin-2/FAS/PPAR γ /FABP4/insulin axis in adipose tissue modulating bone mass and strongly indicates that FAS and Kindlin-2 are new potential targets and C75 or AAV-Rec2-CasRx-sgK2 treatment are potential strategies for OP treatment.

KEY WORDS Kindlin-2; Adipocyte; FAS; Bone homeostasis; AAV-Rec2-CasRx-sgK2; Osteoporosis; C75; mRNA editing

1. Introduction

Osteoporosis (OP), a systemic skeletal disease caused by the imbalance between osteoblast-mediated bone formation and osteoclast-mediated bone resorption¹, primarily affects the elderly population and leads to decreased bone mineral density (BMD) with an increased risk of fracture^{2,3}. OP has continued to be a global public problem, affecting more than 200 million individuals⁴, and about 1 in 3 women and 1 in 5 men over the age of 50 will experience an osteoporotic fracture⁵. At present, there are several FDA-approved drugs for the treatment of OP in the clinic, however, most of them have limitations in side effects or indications and cannot meet the needs of most OP patients. For instance, the use of bisphosphonates, anti-resorptive agents, which used to be the most commonly used drugs for OP treatment^{4,6}, is limited by their severe side effects, including gastrointestinal symptoms, acute phase response, atypical femur fractures and osteonecrosis of the jaw^{7,8}. Denosumab (a monoclonal antibody against RANKL) is another anti-resorptive agent which represses bone resorption significantly but also inhibits bone formation^{9,10}, thus resulting in increased BMD but not improved microarchitecture. That's why Denosumab increases the risk of vertebral fractures within 12 months after discontinuation of the drug¹¹. The use of Teriparatide (parathyroid hormone analogue), another anti-osteoporotic drug approved by FDA, is also limited due to its potential risk of inducing osteosarcoma, and patients with primary or secondary hyperparathyroidism are not suitable for the use of parathyroid hormone (PTH)^{12,13}. Romosozumab (a monoclonal antibody against sclerostin), a recently approved drug for OP treatment by FDA, has the side effect of increasing the risk of cardiovascular disease, and that's why FDA requires a black box warning to be added to the packaging and instructions^{14,15}. Furthermore, according to the results of its

previous clinical trials, romosozumab has a clear preventive effect on vertebral fractures, but the preventive effect on fractures outside the vertebral body is significantly inferior to the former; however, non-vertebral fractures account for more than 85% fractures clinically¹². Therefore, it is of great significance to explore new therapeutic targets and develop new drugs for the treatment of OP that could meet the requirements of most OP patients. Overnutrition or obesity is another global and costly health challenge facing modern society. Among the population of over 18 years old, more than 1.9 billion are overweight or obese. Obesity can lead to a significant increase in the incidence of certain metabolic diseases, including low bone mass disorders, hypertension, diabetes, cardiovascular diseases, etc.^{16,17}. Thus, strategies that could reduce body weight and increase bone mass simultaneously are of great clinical significance.

Adipose tissue is the largest endocrine organ, which regulates central and peripheral systemic metabolism by secreting adipocyte derived peptide hormones, lipid signals, inflammatory factors, and miRNA, etc.¹⁸⁻²³. For example, the activation of PPAR γ , the master transcription factor controlling adipogenesis²⁴, enhances the lipid uptake and storage capacity of adipocytes, so that lipids flow from liver to adipose tissue²⁵. FABP4, a major downstream target of PPAR γ ¹⁶, plays a critical role in modulating β cell function²⁶. FAS, encoded by *Fasn*, a lone enzyme for *de novo* lipogenesis, is essential for PPAR γ activation and FABP4 expression by synthesizing fatty acids²⁷. Specific deletion of FAS in adipocytes results in smaller adipocytes²⁸. It is reported that adipose tissue also plays important roles in regulating bone homeostasis. Extracellular vesicles derived from adipose tissue stem cells exert protective effect on OP through osteoprotegerin and miR-21-5p²⁹. Macrophages of epididymal adipose tissue regulate bone homeostasis through secreting osteopontin³⁰. Blocking β -subunit of follicle-stimulating hormone (FSH) by a polyclonal antibody reduces white adipose tissue, promotes profound beiging and increases bone mass^{31,32}. Adipocyte ablation in adult mice causes massive bone gain³³. Recently, Yang et al.¹⁷ reported that targeting adipocytic DDR2 increases bone mass, improves bone mechanical properties, and resists weight gain caused by high-fat diet (HFD) fed in mice. The above findings suggest that it is feasible to develop new drugs or strategies to prevent bone loss by targeting adipose tissue, and systemic study of the mechanisms through which adipose tissue regulating bone homeostasis could help developing new strategies for treatment

of OP and even obesity, thus decreasing the incidence of certain obesity-related metabolic diseases, such as hypertension, diabetes, cardiovascular diseases, etc.

Kindlin-2, one of the three members of Kindlin family in mammals³⁴, is encoded by *Fermt2* and expressed in various tissues and cells^{34,35}. Kindlin-2 plays critical roles in cell migration, differentiation, and survival through mediating integrin activation³⁶⁻³⁹. Kindlin-2 is crucial for organ development and homeostasis revealed by studies from our group and others, including the heart, kidney, pancreas, bone, and cartilage, and in the occurrence and development of fatty liver and liver fibrosis, etc.⁴⁰⁻⁴⁹. However, the role and mechanisms of adipocyte Kindlin-2 in modulating bone homeostasis remain unclear.

In present study, we aim to demonstrate whether and how adipocyte Kindlin-2 regulates bone homeostasis and whether targeting Kindlin-2 expression in adipocyte could be a potential therapeutic strategy for OP treatment. We demonstrate that Kindlin-2 loss in adipocytes or AAV-Rec2-CasRx-sgK2 mediated RNA editing of *Kindlin-2* in adipocytes both significantly increases bone mass and improves bone mechanical properties. Kindlin-2 deficiency accelerates FAS degradation and thus decreases PPAR γ and FABP4 expression, leading to increased insulin secretion by β cell, increased insulin signaling in bone tissues, and thus increased bone formation. FAS inhibition by C75 markedly increases bone mass in WT C57BL/6 mice. Our work provides potential targets and strategies for OP treatment, which is of great significance.

2. Materials and methods

2.1. Animal studies

To generate *Kindlin-2^{fl/fl}* mice, two loxP sites were inserted from exons 5 and 6 at the *Kindlin-2* locus through homologous recombination, as described in our previous study⁴⁷. The Adipoq-Cre-transgenic mice harboring the *Adipoq-Cre* BAC transgene which expresses Cre recombinase controlled by the adiponectin (*Adipoq*) promoter/enhancer regions within the *BAC* transgene were purchased from the Jackson laboratory⁵⁰. The generation of *Kindlin-2^{fl/fl};Adipoq-Cre* mice, the adipocyte specific Kindlin-2 knockout mice, was previously described⁵¹. Briefly, we bred *Kindlin-2^{fl/fl}* mice with *Adipoq-Cre* mice⁵⁰ and obtained *Kindlin-2^{fl/+};Adipoq-Cre* mice. By further breeding of *Kindlin-2^{fl/+};Adipoq-Cre* mice with *Kindlin-2^{fl/fl}* mice, we obtained *Kindlin-2^{fl/fl};Adipoq-Cre* mice. The Cre-negative *Kindlin-2^{fl/fl}* mice were used as controls in our study. All mice used in current study were maintained in C57BL/6 background through

being crossed with normal C57BL/6 mice for over 10 generations. Mice were group-housed at 20 to 24 °C in a humidity (40%–60%) environment and exposed to a 12-h light/12-h dark cycle. For glucose tolerance test, mice were fasted 16 h before injected with glucose (1 g/kg body weight, i.p.). All protocols for animal studies were approved by the Institutional Animal Care and Use Committee of Southern University of Science and Technology.

2.2. Micro-computerized tomography (μ CT) analysis

Fixed non-demineralized femurs were used for μ CT analysis using a Bruker μ CT (SkyScan 1172 Micro-CT, Bruker MicroCT) according to the standards of techniques and terminology suggested by the American Society for Bone and Mineral Research⁴⁶. Briefly, femurs were scanned at 60 kV, 100 μ A, 926 ms with a resolution of 10 μ m. A region of interest (ROI) of 1.5 mm length starting from 0.5 mm proximal to the distal growth plate was analyzed for trabecular measurements and a ROI of 1.0 mm length of mid-femoral cortical bone was analyzed for cortical bone analysis. All key parameters including the BMD, bone volume/tissue volume fraction (BV/TV), trabecular number (Tb.N), trabecular separation (Tb.Sp) and cortical thickness (Crot.Th) were analyzed.

2.3. Mineral apposition rate (MAR), mineralizing surface per bone surface (MS/BS), and bone formation rate (BFR) determination

Calcein double labeling experiment was performed as we previously described^{48,52}. Briefly, mice were injected intraperitoneally with calcein (Sigma, cat# C0875) at a dosage of 20 mg/kg at 7 and 2 days before sacrifice. Femurs were isolated and fixed with 70% ethanol, then non-demineralized femurs were embedded with Osteo-Bed Bone Embedding kit (Sigma, cat# EM0200) following the manufacturer's instruction and sectioned at 5 μ m. Images were captured using a fluorescence microscope (Olympus-BX53) and used for the MAR, MS/BS, and BFR evaluation as previously described⁵³.

2.4. Colony forming unit-fibroblast (CFU-F) assay and Colony forming unit-osteoblast (CFU-OB) assay

The CFU-F and CFU-OB assay were conducted as we previously described⁵³. Bone marrow nucleated cells isolated from 5-month-old mice were seeded in a 12-well plate at a cell density of 1×10^6 cells/well. For CFU-F assay, the cells were cultured in the

Mouse MesenCult Proliferation Medium (STEMCELL Technologies, cat# 05513) for 14 days, then Giemsa staining (Sigma, GS500) was performed according to the manufacturer's protocol. For CFU-OB assay, the cells were cultured in differentiation medium (*i.e.*, α -MEM containing 10% fetal bovine serum (FBS), 50 μ g/mL L-ascorbic acid and 2 mmol/L β -glycerophosphate) for 21 days, then alizarin red staining was performed.

2.5. *In vitro* and *in vivo* osteoclast differentiation assay

In vitro osteoclast formation assay was performed as we previously described⁵⁴. Tartrate-resistant acid phosphatase (TRAP) staining of decalcified tibia sections from both control and K2KO mice was performed as we previously described⁴⁶. The osteoclast surface and osteoclast number were measured as we previously described⁵⁵.

2.6. *In vitro* osteoblastic and adipogenic differentiation of bone marrow stromal cells (BMSCs)

Primary BMSCs, isolated from femurs and tibias of 5-month-old mice, were cultured as we previously described⁵². BMSCs were seeded in 6-well plate at the density of 5×10^5 cells/well and cultured in osteogenic medium (*i.e.*, α -MEM containing 10% FBS and 50 μ g/mL ascorbic acid) for 7 days followed by quantitative real-time RT-PCR (RT-qPCR) analysis or Western blot (WB) analysis to determine the expression of osteogenic genes, or alkaline phosphatase (ALP) staining. For *in vitro* adipogenic differentiation assay, the above primary BMSCs were cultured with adipogenic differentiation medium (MesenCult Adipogenic Differentiation Kit, Stemcell Technologies) for 7 days, followed by RT-qPCR or WB analyses, or cultured for 14 days, followed by oil red O (Sigma, O1391-250ml) staining as we previously described⁵².

2.7. RT-qPCR and WB analyses

RT-qPCR analysis was performed as previously described⁵⁵. 1 μ g of RNA, isolated using the RNeasy Mini Kit (Qiagen, Cat#74104) according to the manufacturer's instruction, was reverse transcribed after being denatured, in a reaction system with a total volume of 25 μ L containing 100 pmol of random hexamers (Applied Biosystem, Foster, CA, USA) and 12.5 U MultiScribe reverse transcriptase (Applied Biosystem, Foster, CA, USA). RT-qPCR analysis was used to determine the relative mRNA levels

using the SYBR Green kit (Bio-Rad Laboratories Inc, Germantown, MD, USA). The mRNA levels of each detected gene were normalized to *Gapdh* expression. The DNA sequences of primers used for RT-qPCR in this study are listed in Supporting Information Table S1. WB analysis was performed as previously described⁵⁶. Briefly, protein samples were fractionated on a 10% SDS-PAGE gel and transferred onto nitrocellulose membranes (Schleicher & Schuell, Keene, NH, USA). The membrane was blocked using 5% nonfat milk in Tris-buffered saline/Tween 20 buffer, after that, the membrane was firstly probed with primary antibodies, then secondary antibodies with the conjugation of horseradish peroxidase, finally the membrane was visualized using a Western Blotting Detection Kit (GE Healthcare, cat#: RPN2106). Primary and secondary antibodies used in this study are listed in Supporting Information Table S2.

2.8. ELISA assay of serum procollagen type 1 amino-terminal propeptide (P1NP), collagen type I cross-linked C-telopeptide 1 (CTX1), FABP4, insulin

ELISA assay was conducted as we previously described. Briefly, serum samples were isolated from blood collected from control and K2KO mice. Serum P1NP, CTX1, FABP4 and insulin were measured by using P1NP ELISA kit (Immunodiagnostic Systems Limited, cat# AC-33F1), CTX1 ELISA kit (Immunodiagnostic Systems Limited, cat# AC-06F1), FABP4 ELISA kit (Beyotime Limited, cat# SEKH-0169-96T), and insulin ELISA kit (Beyotime Limited, cat# SEKH-0219-96T), respectively, according to the manufacturers' instructions.

2.9. Immunohistochemistry (IHC) and immunofluorescence (IF) staining

IHC and IF staining were performed as we previously described. For IHC staining, 5 μ m sections were stained with indicated antibodies or control normal IgG using the EnVision+System-HRP (DAB) kit (Dako North America Inc, Carpinteria, CA, USA) according to the manufacturer's instruction⁴⁵. The following antibodies were used for IHC staining in this project: osterix (OSX) and phosphorylated insulin receptor substrate-1 (pIRS1). For IF staining, 5 μ m paraffin sections were stained with indicated antibodies as we previously described^{45,57,58}. The following antibodies were used for IF staining in this project: osteocalcin (OCN) and insulin. The fluorescence signal was acquired by Nikon Confocal A1R system under 20 \times objective lens.

2.10. AAV-Rec2-CasRx-sgK2 construction and injection

CasRx mediated RNA editing was designed and performed as previously described⁵⁹. For sgRNA screening, 5 sgRNAs targeting mouse *Kindlin-2* mRNA was constructed into pXR003 and co-transfected with pXR001 to evaluate RNA editing efficiency. SgRNA4 (5'-ACGTGTCTTTGAAAGTGCACCAG-3') and sgRNA5 (5'-TAGTACTTGAATCGGAGCAGCAA-3') were used for further study according to their high knockdown efficiency. AAV-Rec2 carrying a *CasRx* gene under *Adipoq* promoter and sgRNA4 under *U6* promoter was synthesized by Vigene Biosciences (Jinan, Shandong, China). For *in vivo* study, 3-month-old WT C57BL/6 mice were intraperitoneally injected with AAVs at a dose of 1×10^{10} vg/mouse in 150 μ L of AAV dilution buffer⁶⁰. After 2 months of injection, mice were sacrificed for further evaluation.

2.11. DNA constructs and transfection

We obtained the negative control and mouse-specific *Kindlin-2* siRNAs from Suzhou GenePharma Co., Ltd. (Suzhou, China). The mouse negative control siRNA sequence is: 5'-UUCUCCGAACGUGUCACGUTT-3', the mouse *Kindlin-2* siRNA sequence is: 5'-GCUUCUAUGCAGAGC GCUUTT-3'.

2.12. Human serum samples

Serum samples from healthy individuals and OP patients were obtained in Nanjing Drum Tower Hospital (Nanjing China) with procedures approved by the ethics committee of the Drum Tower Hospital (IRB No: 2021-192). Written informed consents were provided by all participants. Bone mineral density of the participants was measured, those with T scores ≤ -2.5 were assigned to the OP group, and those with T scores ≥ -1 were assigned to the control group⁶¹ (Supporting Information Table S3). Those participants with other metabolic diseases, including diabetes, arthritis, osteonecrosis, etc., were excluded from this study.

2.13. Statistical analyses

Mice used in this study were grouped randomly. Unpaired Student's *t* test (two groups) or one-way ANOVA, and two-way ANOVA (multiple groups), followed by Tukey's *post hoc* test as appropriate, were used for data analysis. Results are expressed as mean \pm standard deviation (SD), as indicated in figure legends. Differences with $P < 0.05$ were considered of statistically significance.

3. Results

3.1. Deleting *Kindlin-2* in adipocytes dramatically increases systemic bone mass and improves bone mechanical properties in mice

To study the age-related change and HFD-related change in adipocyte *Kindlin-2*, we firstly determined its expression in white adipose tissue (WAT) from young (5-month-old) and aged (18-month-old) mice, normal chow diet (NCD) fed and HFD fed mice. IF staining revealed that *Kindlin-2* expression was markedly up-regulated in epididymal WAT (eWAT) and inguinal WAT (iWAT)) from aged or HFD fed mice (Supporting Information Fig. S1A–S1C) who had lower bone mass than young or NCD fed mice (Fig. S1D–S1F). These results indicate that decreased bone mass is accompanied by elevated *Kindlin-2* expression in white adipose tissue during aging and HFD. These results aroused our interest in investigating the role of adipocyte *Kindlin-2* in maintaining bone homeostasis. For this purpose, we generated *Kindlin-2^{fl/fl};Adipoq-Cre* mice (hereafter referred to as K2KO). WB analysis revealed that *Kindlin-2* expression in eWAT from K2KO mice was significantly reduced, but not in bone tissue, compared with that of control mice (Fig. S1G). μ CT analysis of distal femurs, calvariae and vertebrae revealed a high bone mass phenotype of both genders and different ages of K2KO mice compared with that of control mice (Fig. 1A–J). The BMD and BV/TV of distal femurs in male K2KO mice were increased by 39.67% and 57% respectively at 5 months of age, 55% and 90% respectively at 12 months of age (Fig. 1B and C). The bone mass increase was even more significant in female K2KO mice. The BMD and the BV/TV of distal femurs in female K2KO mice were increased by 128% and 203%, respectively, at 5 months of age compared with control littermates (Fig. 1B and C). Both genders of K2KO mice displayed markedly increased Tb.N (Fig. 1D), and drastically decreased Tb.Sp (Fig. 1E). A significant increase of Cort.Th was observed in distal femurs of both genders of K2KO mice, it was increased by 14% in male mice and 25% in female mice at 5 months of age (Fig. 1F). *Kindlin-2* loss also caused a significant increase of bone mass in calvariae (Fig. 1G and H) and vertebrae (lumber spine (L4)) (Fig. 1I and J). μ CT analysis revealed that, in male mice at 5 and 12 months of age, the BV/TV of calvariae was increased by 15% and 13%, respectively, 82% and 32% in vertebrae, respectively. In female mice at 5 months of age, the BV/TV of calvariae and vertebrae was increased by 34% and 155%, respectively (Fig. 1H and J). Since bone mass increase is much more obvious in female mice, we only used female

mice in the following experiments of this study to minimize the use of mice and keep consistency.

There is a tight crosstalk between muscle tissue and bone tissue, the strength of skeletal muscle could affect bone mass profoundly^{62,63}. Therefore, we tested the gripping power of the front paws of 5-month-old mice. Results showed that Kindlin-2 deletion in adipocyte slightly increased the gripping power but with no significance (Supporting Information Fig. S2B) at this age with similar body weight (Fig. S2A).

We applied the 3-point bending tests on femurs of 5-month-old control and K2KO mice to examine whether Kindlin-2 loss in adipocytes affects the mechanical properties of bone tissue (Fig. 1K). As presented in Fig. 1, femurs from K2KO mice had higher maximum load (Fig. 1L) and stiffness (Fig. 1N) with no alterations in maximum displacement (Fig. 1M) than control mice. The average maximum load of femurs from 5-month-old control mice was 18.2 N, and this number was increased to 25.3 N, increased by 39%. The average stiffness was 79.7 N/mm in control mice and 120.1 N/mm in K2KO mice, increased by 63.7%.

Collectively, these results demonstrate that adipocyte Kindlin-2 functions as a crucial regulator of bone homeostasis.

Insert Fig. 1

3.2. Kindlin-2 loss markedly increases osteoblast formation and bone-forming activity while has relatively mild effects on osteoclast formation and bone resorption

Since bone homeostasis is maintained by the balance between osteoclast-mediated bone resorption and osteoblast-mediated bone formation, we investigated osteoclast formation and bone resorption *in vivo* and *in vitro* firstly. The result of TRAP staining of tibial sections revealed that Kindlin-2 loss had no significant effect on osteoclast formation *in vivo* both in 5-month-old and 12-month-old mice, indicated by similar osteoclast number/bone perimeter (Oc.Nb/BPm) and osteoclast surface/bone surface (Oc.S/BS) in both primary and secondary spongiosa bones (Supporting Information Fig. S3A–S3E). ELISA assay of the serum levels of the CTX1, derived from type I collagen during *in vivo* osteoclast mediated bone resorption, showed a slight but significant increase of average value in K2KO group (Fig. S3F), this could be due to an increase in the total number of osteoclasts. *In vitro* osteoclast differentiation assay displayed that the number of multinucleated TRAP positive osteoclasts was similar in both control and K2KO groups (Fig. S3G and S3H), indicating that the capacity of bone marrow

monocytes (BMMs) differentiating into osteoclasts was not much changed by Kindlin-2 loss in adipocytes. Thus, Kindlin-2 deletion in adipocytes has no obvious effect on osteoclast formation and bone resorption.

We next investigated whether osteoblast formation and function were altered by Kindlin-2 loss. The calcein double labeling experiments revealed a significant increase in osteoblast bone-forming activity *in vivo* of K2KO mice, indicated by dramatic increases in MAR, MS/BS, and BFR in the femoral metaphyseal cancellous bones and cortical bones (Fig. 2A–G). Von Kossa staining of undecalcified femoral sections displayed marked increases in osteoid volume/tissue volume (OV/TV) and mineralized BV/TV of the cancellous bones of K2KO mice compared with control mice (Fig. 2H–J). ELISA assay showed a significant increase of P1NP (an *in vivo* marker of osteoblast bone-forming activity) in serum of K2KO mice compared with that of control mice (Fig. 2K). The number of cuboidal osteoblasts that are active for bone formation on trabecula surfaces was greatly increased in K2KO mice compared with control littermates, while the number of flat osteoblasts which are inactive for bone formation was not obviously changed (Fig. 2L–N). IHC staining revealed that the number of OSX-positive cells (*i.e.*, pre-osteoblasts) located on the tibial metaphyseal cancellous bone surface was drastically increased in K2KO mice relative to that in the control mice (Fig. 2O and Q). The results of IF staining showed that the number of OCN-positive cells (*i.e.*, mature osteoblasts) was also significantly increased by Kindlin-2 loss in adipocytes (Fig. 2P and R). Thus, Kindlin-2 deletion in adipocytes significantly increases osteoblast differentiation and bone formation.

Insert Fig. 2

3.3. Kindlin-2 loss increases osteogenic while decreases adipogenic differentiation of BMSCs

To determine the underlying mechanism(s) for increased osteoblast formation in K2KO mice, we performed the CFU-F assays and CFU-OB assays using freshly flushed out primary bone marrow cells from 5-month-old K2KO mice and control littermates. Results showed that Kindlin-2 loss dramatically increased the numbers of CFU-F (Fig. 3A and B) and CFU-OB (osteoprogenitors) colonies (Fig. 3C and D) by 168% and 155%, respectively. RT-qPCR analyses using RNA isolated from bone tissues or fresh bone marrow of control and K2KO mice revealed that the expression of osteogenic genes, including *Runx2*, *Osx*, *Colla1*, *Alp*, etc., were significantly elevated by Kindlin-

2 deletion (Fig. 3E and F). We further determined whether Kindlin-2 deficiency altered the *in vitro* differentiation capacity of primary BMSCs. Results showed that the mineralization (Fig. 3G and H) and osteoblast gene expression (Fig. 3I–K) were both greatly increased in K2KO group compared with those in control group, the expression of RUNX2, OSX, ALP were all significantly increased both at RNA and protein levels. *In vitro* adipogenic differentiation of BMSCs isolated from K2KO mice was severely impaired compared with that of control mice as measured by Oil Red O staining (Fig. 3L and M). Consistently, Kindlin-2 loss dramatically decreased the mRNA expression of adipogenic differentiation genes, including those encoding FABP4 and leptin, but not PPAR γ or FAS (Fig. 3N). The protein level of FAS, PPAR γ , FABP4 and leptin, were severely downregulated by Kindlin-2 loss revealed by WB analyses using protein extracts isolated from BMSCs after being adipogenic-differentiated (Fig. 3O and P). Furthermore, the number of adipocytes in bone marrow was also significantly reduced in K2KO mice revealed by hematoxylin and eosin (H&E) staining (Fig. 3Q–S).

Insert Fig. 3

3.4. Kindlin-2 loss decreases FABP4 and increases insulin signaling

FABP4, also known as aP2, a major target gene of PPAR γ ^{64,65}, negatively regulates β cell mass and function²⁶. WB analyses revealed that Kindlin-2 loss resulted in a significant reduction of FABP4 in BMSCs after being adipogenic-differentiated (Fig. 3N–P). Based on this finding, together with the observation that the glucose tolerance was slightly improved in both genders of K2KO mice at different ages compared with that of control littermates (Supporting Information Fig. S4A), we next determined insulin expression and insulin signaling in K2KO mice. As expected, ELISA assay revealed a significant decrease of FABP4 (Fig. 4A) and a dramatic increase of insulin in serum (Fig. 4B) obtained from K2KO mice compared with that of control group. IF staining also displayed an increase of insulin expression in islet (Fig. 4C and D) in K2KO mice. Consistent with the increased serum insulin level, IHC staining of tibial cross sections showed drastically increased expression of pIRS1, a key member of insulin signaling pathway, in K2KO mice (Fig. 4E and F). And as expected, the phosphorylated ribosomal S6 kinase (pS6K), a key downstream factor of pIRS1, was also significantly increased in K2KO bone tissues (Fig. 4E and G). What's more, treatment with serum from K2KO mice markedly increased pIRS1 and osteogenic

markers, including RUNX2, OSX, ALP, in *in vitro* osteogenic-differentiated BMSCs compared with that of control group (Fig. 4H and I).

We also tested if FABP4 has a direct role on osteoblast formation. WB displayed that osteogenic differentiation of BMSCs was not affected by recombinant mouse FABP4 (rmFABP4) represented by unaltered expression of osteogenic marker genes, including RUNX2, OSX and ALP (Fig. 4J and K).

We then compared the serum level of FABP4 and insulin in OP patients (T -scores ≤ -2.5) and normal control (T -scores ≥ -1). Results showed that serum level of FABP4 was significantly increased (Fig. 4L) while insulin level was decreased in OP patients (Fig. 4M), indicating the potential correlation between the serum levels of FABP4, insulin, and bone mass in human beings.

Insert Fig. 4

3.5. Increased FABP4 expression by rosiglitazone activation of PPAR γ reverses the high bone mass phenotype of K2KO mice

Since FABP4 is a major target gene of PPAR γ , PPAR γ activation increases FABP4 expression. If Kindlin-2 loss increased bone mass through decreased FABP4 expression, then increased FABP4 expression through PPAR γ activation by synthetic ligand rosiglitazone should be able to reverse at least partially the high bone mass in K2KO mice. Therefore, we administered 3-month-old mice with rosiglitazone (30 mg/kg/day) or vehicle (1% carboxymethylcellulose in saline) daily, by oral gavage for 1 month^{66,67}. As expected, results of μ CT analysis displayed a decrease of bone mass in control mice after rosiglitazone treatment. The high bone mass phenotype caused by Kindlin-2 deletion was reversed by rosiglitazone treatment (Fig. 5A–C). Rosiglitazone treatment did not change Kindlin-2 and FAS (Supporting Information Fig. S8A) but significantly increased PPAR γ expression in WAT in both groups (Fig. 5D–F). Furthermore, the decreased serum FABP4 level in K2KO mice was also reversed by rosiglitazone treatment examined by ELISA assay (Fig. 5G). And as expected, the increased insulin level both in serum (Fig. 5H) and in islet (Fig. 5I and J) were decreased by rosiglitazone treatment revealed by ELISA assay and IF staining. Furthermore, the increased pIRS1 in bone tissues in K2KO mice was also largely reversed by rosiglitazone treatment (Fig. 5K and L).

Numerous studies have revealed a positive relationship between insulin signaling and bone mass⁶⁸⁻⁷⁴. Taken together, the above results demonstrate that adipocyte Kindlin-2 modulates bone mass at least partially through regulating FABP4/insulin signaling, and increased insulin signaling caused by decreased FABP4 makes crucial contribution to the high bone mass of K2KO mice.

3.6. Kindlin-2 controls PPAR γ and FABP4 expression through modulating FAS protein level in adipocytes

Next, we determined how Kindlin-2 loss in adipocytes decreases FABP4 expression. Since PPAR γ controls FABP4 expression, and deletion of Kindlin-2 in adipocytes resulted in dramatically decreased PPAR γ expression (Fig. 3O and P, Fig. 5D and F), we tested if Kindlin-2 regulates FABP4 expression through modulating PPAR γ . We firstly conducted co-immunoprecipitation (co-IP) assays using antibodies against Kindlin-2 and PPAR γ respectively. However, we were not able to demonstrate an interaction between Kindlin-2 and PPAR γ (Supporting Information Fig. S5A and S5B), indicating that Kindlin-2 modulates PPAR γ expression indirectly.

Insert Fig. 5

FAS, encoded by *Fasn*, is the lone enzyme for *de novo* lipogenesis⁷⁵, and is critical for PPAR γ activation and expression⁷⁶. Results showed that the protein level but not mRNA level of FAS was dramatically reduced by Kindlin-2 loss in BMSCs after being adipogenic-differentiated (Fig. 3N–P), and FAS was downregulated in K2KO eWAT revealed by IF staining (Fig. S8A). It is reported that FAS deletion in adipocyte results in reduced adipocyte size²⁸. Indeed, the decreased FAS expression by Kindlin-2 loss also decreased white adipocyte size and resulted in smaller adipocyte (Supporting Information Fig. S6A and S6B), however, the cell size of brown adipocyte tissue (BAT) was not much changed by Kindlin-2 loss (Fig. S6C). We next determined if Kindlin-2 controls PPAR γ and FABP4 expression through modulating FAS expression in adipocytes. Kindlin-2 knockdown by siRNA markedly decreased FAS, PPAR γ and FABP4 protein level. The decrease of PPAR γ and FABP4 protein level caused by Kindlin-2 knockdown could be blocked by FAS overexpression (Fig. 6A). Kindlin-2 overexpression elevated FAS, PPAR γ and FABP4 protein level. The increase of PPAR γ and FABP4 protein level caused by Kindlin-2 overexpression could be blocked by FAS

inhibitor C75⁷⁷ (Fig. 6B). The above results defined a novel Kindlin-2/FAS/PPAR γ /FABP4 axis in adipocyte *in vitro*.

3.7. Kindlin-2 modulates FAS stabilization through regulating its ubiquitination

Results of IF staining of 3T3-L1 preadipocytes using antibodies against Kindlin-2 and FAS revealed that both Kindlin-2 and FAS were widely distributed all over the cytoplasm. A strong colocalization of Kindlin-2 and FAS was observed in the cytoplasm (Fig. 6C). We next determined if Kindlin-2 interacts with FAS by performing co-IP assays using whole-cell extracts isolated from 3T3-L1 preadipocytes. Results showed that a strong signal of FAS protein could be detected in the Kindlin-2 immunoprecipitates, vice versa (Fig. 6D), indicating an interaction of the endogenous Kindlin-2 and FAS proteins. Same results were confirmed in HEK293T cell line (Supporting Information Fig. S7A and S7B). We then determined if Kindlin-2 knockdown affects FAS protein stability by conducting the cycloheximide (CHX) experiments. We found that *KINDLIN-2* knockdown dramatically promoted the FAS protein degradation in 3T3-L1 preadipocytes (Fig. 6E and F). MG132 treatment resulted in dramatically increased FAS accumulation and blocked the decrease of FAS caused by Kindlin-2 knockdown (Fig. 6G and H), indicating that FAS is degraded mainly through the proteasomal degradation pathway. Next, we determined whether *KINDLIN-2* can modulate the proteasome-mediated degradation of FAS protein by analyzing the polyubiquitination level of FAS protein. Results displayed that *KINDLIN-2* overexpression greatly decreased the level of FAS polyubiquitination in HEK293T cells (Fig. 6I).

Collectively, these results suggest that Kindlin-2 regulation of PPAR γ expression is FAS dependent. Kindlin-2 loss promotes proteasome-mediated degradation of FAS protein, leading to decreased PPAR γ activation and FABP4 expression, which finally increases insulin secretion (Fig. 6J). Thus, PPAR γ and FABP4 functions downstream of FAS. Rosiglitazone treatment increased PPAR γ activation without changing FAS expression (Supporting Information Fig. S8A), further demonstrating the above conclusion.

Insert Fig. 6

3.8. FAS inhibitor C75 treatment increases bone mass of C57BL/6 mice

To further verify the mechanisms established in this study, we injected 3-month-old WT C57 mice with FAS inhibitor C75 intraperitoneally every 3 days for 1 month, at a dose of 10 mg/kg. The body weight was not changed by C75 treatment (Supporting Information Fig. S9A). The mass of iWAT and eWAT were significantly decreased by C75 treatment, while the mass of BAT was not affected (Fig. S9B). μ CT analysis of distal femurs showed that the bone mass in mice treated with C75 was greatly elevated compared with vehicle group (Fig. 7A). Both BMD (Fig. 7B) and BV/TV (Fig. 7C) were significantly increased in C75 treated group compared with control group. H&E staining also revealed an increase of trabecular bone mass in mice treated with C75 (Fig. S9C). Serum level of P1NP was also greatly increased by C75 treatment revealed by ELISA assay (Fig. 7F). IF staining demonstrated an elevated signal of OCN in bone tissues of mice with C75 treatment compared with control group (Fig. 7D and E). IF staining of eWAT revealed significant decrease of FAS, PPAR γ and FABP4 while Kindlin-2 expression was not altered by C75 treatment (Fig. 7G and H). The decrease of FABP4 was further demonstrated by ELISA assay of the serum (Fig. 7I). These results suggest that FAS functions upstream of PPAR γ and FABP4, downstream of Kindlin-2. IF staining of the islet (Fig. 7J and K) and ELISA assay of the serum (Fig. 7L) both displayed the increase of insulin level. Accordingly, pIRS1 expression in bone tissues of mice treated with C75 was greatly elevated (Fig. 7M and N). Since myeloid cells also express low level of FAS, we examined if osteoclast formation is affected by C75 treatment. TRAP staining of tibiae sections displayed that osteoclast formation was not affected by C75 treatment (Fig. S9D). To determine the biosafety of the concentration of C75 used in this study, we examined the histological changes of heart, kidney, liver, lung and spleen by H&E staining. Results showed that all organs examined showed normal tissue and cell structure after C75 treatment compared with that of control group (Fig. S9E), suggesting that the concentration of C75 used in this study is of great biosafety in mice. Collectively, intraperitoneal injection of FAS inhibitor C75 phenocopies the effect of Kindlin-2 deletion in adipocytes and increases bone mass, indicating that FAS is a potential therapeutic target and C75 is a potential drug for the treatment of diseases with bone loss, including OP.

Insert Fig. 7

3.9. AAV-CasRx mediated RNA editing of KINDLIN-2 in adipocytes increases bone mass of WT C57BL/6 mice

To further determine whether the mechanisms of this study have a potential translational significance, we then determined if *KINDLIN-2* knockdown *via* AAV increases bone mass⁶⁰. Rec2 is an adipose targeting AAV serotype which improves the tissue specificity through restricting the off-target transduction in liver⁶⁰. We first screened five sgRNAs for their efficiency in CasRx mediated RNA editing of *Kindlin-2* in 3T3-L1 preadipocytes. Results showed that co-transfection of a vector containing CasRx gene with sgRNAs 4 and 5 that target *Kindlin-2* mRNA, resulted in 78.4% and 77.3% ($n = 3$ repeats) reduction of *Kindlin-2* protein respectively (Supporting Information Fig. S10A and S10B). We next examined whether *Kindlin-2* knockdown in adipocytes *in vivo* by using CasRx-induced RNA editing could increase bone mass. We constructed AAV-Rec2-CasRx-sgK2 (Rec2-sgK2) driven by the *Adipoq* promoter to knockdown *Kindlin-2* through RNA editing specifically in adipose tissue, and AAV-Rec2-CasRx-sgNC (Rec2-sgNC) carried an sgRNA that has no known targeting gene as a control. The design of Rec2-sgK2 is illustrated in Fig. 8A. Next, we tested the effect of Rec2-sgK2 on bone mass accrual. 3-month-old C57BL/6 mice were intraperitoneally injected with Rec2-sgK2 or Rec2-sgNC. After 2 months, mice were sacrificed, and specimens were collected. *Kindlin-2* knockdown efficiency in WAT and other organs was evaluated by WB. Results showed that Rec2-sgK2 injection dramatically decreased *Kindlin-2* expression in eWAT, but not in other tissues (Fig. S10C and S10D). *Kindlin-2* knockdown reduced eWAT mass (Fig. S10F) without affecting the body weight (Fig. S10E) at this time point. μ CT analysis of distal femurs showed a significant increase of bone mass (Fig. 8B), BMD (Fig. 8C) and BV/TV (Fig. 8D) were both significantly increased in Rec2-sgK2 treated mice compared with that of Rec2-sgNC treated mice. H&E staining also displayed an increase of trabecular bone in tibiae from Rec2-sgK2 treated mice (Fig. S10G). Serum level of P1NP was also greatly increased in Rec2-sgK2 treated mice revealed by ELISA assay (Fig. 8E), suggesting increased *in vivo* osteoblast-mediated bone formation activity. IF staining displayed a significantly enhanced signal of OCN in bone tissues of Rec2-sgK2 treated mice, indicating that osteoblast formation was promoted (Fig. 8F and G). Rec2-sgK2 treatment also dramatically reduced the level of FAS, PPAR γ , FABP4 in eWAT (Fig. 8H and I). Decreased serum level of FABP4 (Fig. 8J) and increased expression of insulin evaluated by ELISA assay (Fig. 8M) or by IF staining (Fig. 8K and L), together with strengthened pIRS1 signal in bone tissues (Fig. 8N and O), indicated the elevated insulin signaling in mice treated with Rec2-sgK2. Collectively, these results

demonstrate that adipocyte *KINDLIN-2* is a potential therapeutic target and AAV-mediated RNA editing is a potential strategy for OP treatment.

Insert Fig. 8

4. Discussion

In this study, by using a strategy that combines gain- and loss-of function approaches, we for the first time demonstrate that Kindlin-2 through its expression in adipocytes plays a crucial role in controlling bone homeostasis. Specific inhibition of Kindlin-2 in adipocytes dramatically increases bone mass of distal femurs, vertebrae and calvariae, both in cancellous and cortical bones. Furthermore, the mechanical properties of long bones are significantly improved by Kindlin-2 deletion.

One major finding of this study is the demonstration that Kindlin-2 plays key roles in adipose tissue regulating bone homeostasis. Several lines of evidence from the current study support this notion. First, Kindlin-2 expression increases in WAT in an age-related manner and is accompanied by decreased bone mass. Second, specific Kindlin-2 deletion in adipocytes increases bone mass and improves mechanical properties of bone tissue. Finally, Kindlin-2 knockdown in adipose tissue *via* intraperitoneal injection of AAV-Rec2-CasRx-sgK2 increases bone mass in WT C57BL/6 mice. These findings provide strong evidences that Kindlin-2 in adipocytes could be a potential therapeutic target for bone loss related diseases, such as OP.

In this study, we demonstrate that adipocyte Kindlin-2 regulates bone homeostasis by controlling FAS-dependent PPAR γ -mediated FABP4 expression and insulin signaling. First, the protein level of FAS, a critical enzyme for *de novo* lipogenesis which is important for PPAR γ activation and its downstream FABP4 expression^{76,78-80}, is significantly reduced by Kindlin-2 deletion. Consistently, expression of PPAR γ and FABP4 are dramatically decreased, and insulin signal in both serum and islet in K2KO mice are accordingly elevated. The markedly elevated insulin signaling pathway in bone tissues demonstrated by enhanced pIRS1 and pS6K signals at least partially explains the high bone mass phenotype of K2KO mice based on the well characterized positive effects of insulin signaling pathway in promoting bone mass and bone mechanical property^{68,71,73,81,82}. Second, BMSCs treated with serum obtained from K2KO mice show elevated insulin signaling and increased osteogenic differentiation capacity compared with that of control group, further demonstrating that insulin

signaling is strengthened in K2KO mice. Finally, PPAR γ activation by rosiglitazone reverses the decreased FABP4 and increased insulin expression, and thus reverses the high bone mass phenotype of K2KO mice. Interestingly, consistent with these findings, serum level of FABP4 is increased and insulin is decreased in OP patients revealed by ELISA assay in this study.

Notably, in the present study, we identify Kindlin-2 as a crucial factor controlling PPAR γ expression through modulating FAS protein stability in adipocytes for maintenance of bone homeostasis by *in vivo* and *in vitro* studies. First, both K2KO mice and Rec2-sgK2 treated mice show decreased level of FAS, PPAR γ and FABP4 and increased bone mass. Second, FAS inhibitor C75 treatment reduces PPAR γ and FABP4 protein level while Kindlin-2 expression is unaltered in eWAT, and bone mass is increased. Third, PPAR γ activation by rosiglitazone increases PPAR γ and FABP4 expression but not Kindlin-2 or FAS expression and reverses the high bone mass phenotype of K2KO mice. Finally, *in vitro* studies show that the decrease of PPAR γ protein caused by KINDLIN-2 knockdown in 3T3-L1 preadipocytes is blunted by FAS overexpression, and the increase of PPAR γ by Kindlin-2 overexpression is reversed by FAS inhibition. Thus, we demonstrate the axis of Kindlin-2/FAS/ PPAR γ /FABP4 in adipose tissue that is critical for maintaining bone homeostasis.

We define a mechanism through which Kindlin-2 deletion reduces FAS protein level in adipocytes. Results show that Kindlin-2, through its interaction with FAS, stabilizes FAS protein by inhibiting its polyubiquitination and degradation. Loss of Kindlin-2 accelerates FAS polyubiquitination and degradation.

5. Conclusions

In summary, the current study for the first time demonstrates the role of Kindlin-2 in adipocytes in maintaining bone homeostasis through modulating FAS/PPAR γ /FABP4/insulin axis. This pathway may of great clinical significance for the prevention and treatment of low bone mass related diseases, such as OP. First, RNA editing of Kindlin-2 in adipose tissue *via* intraperitoneal injection of Rec2-sgK2 increases bone mass of C57BL/6 mice, indicating that adipocyte Kindlin-2 is a potential target and Rec2-sgK2 treatment is a potential strategy for OP treatment. Second, intraperitoneal injection of FAS inhibitor C75⁸³, also significantly increases bone mass of WT C57BL/6 mice. FAS inhibitors have been reported with potential clinical application prospects, including the treatment of cancers, nonalcoholic steatohepatitis,

sepsis, etc.^{75,83-85}. Our study lays the foundation for the use of C75 for the treatment of diseases associated with bone loss.

We must acknowledge that there are several limitations in this study. First, while our results show that Kindlin-2 loss accelerates the proteasome degradation of FAS mediated by ubiquitination, it remains to be determined which E3 ligase is required for FAS ubiquitination. Second, in current study, the long-term positive effect of Rec2-sgK2 and FAS inhibitor C75 on bone mass accrual remains to be determined. Third, it remains to be determined if adipocyte Kindlin-2 knock-in mice can lead to the same conclusion of this study. Although the *in vitro* cell experiments show that Kindlin-2 knockdown or overexpression in 3T3-L1 preadipocytes lead to opposite results, *i.e.*, Kindlin-2 knockdown leads to decreased while Kindlin-2 overexpression leads to increased protein level of FAS, PPAR γ and FABP4, we still cannot conclude that Kindlin-2 overexpression in adipocyte could result in bone mass loss in mice. We plan to conduct these experiments in our future study.

Acknowledgments

We acknowledge the assistance of Core Research Facilities of Southern University of Science and Technology. Support of this work partially came from National Natural Science Foundation of China Grants (82022047 and 81972100), the National Key Research and Development Program of China Grants (2019YFA0906001), Guangdong Provincial Science and Technology Innovation Council Grant (2017B030301018).

Author contributions

Study design: Wanze Tang, Guixing Ma and Huiling Cao. Study conducts, data collection and analysis: Wanze Tang, Zhen Ding, Huanqing Gao, Qinnan Yan, Dazhi Yang, Guixing Ma, Xiaoting Hou, Yingying Han, Zhengwei Liu, Litong Chen, Jingping Liu and Huiling Cao. Data interpretation: Huiling Cao, Wanze Tang, Guixing Ma, Dazhi Yang, Zhen Ding, Huanqing Gao and Qinnan Yan. Drafting the manuscript: Huiling Cao, Guixing Ma and Wanze Tang. Dazhi Yang, Guixing Ma and Huiling Cao take the responsibility for the integrity of the data analysis.

Conflicts of interest

The corresponding authors Huiling Cao and Guixing Ma have filed a patent application (202210877899.X) for the treatment of OP. The other authors declare no conflicts of interests.

References

- 1 Abuna RP, Almeida LO, Souza AT, Fernandes RR, Sverzut TF, Rosa AL, et al. Osteoporosis and osteoblasts cocultured with adipocytes inhibit osteoblast differentiation by downregulating histone acetylation. *J Cell Physiol* 2021; **236**: 3906-17.
- 2 Hsieh CI, Zheng K, Lin C, Mei L, Lu L, Li W, et al. Automated bone mineral density prediction and fracture risk assessment using plain radiographs *via* deep learning. *Nat Commun* 2021; **12**: 5472.
- 3 Stone KL, Seeley DG, Lui LY, Cauley JA, Ensrud K, Browner WS, et al. BMD at multiple sites and risk of fracture of multiple types: long-term results from the study of osteoporotic fractures. *J Bone Miner Res* 2003; **18**: 1947-54.
- 4 Ebeling PR, Nguyen HH, Aleksova J, Vincent AJ, Wong P, Milat F. Secondary osteoporosis. *Endocr Rev* 2022; **43**: 240-313.
- 5 Reginster JY, Burlet N. Osteoporosis: a still increasing prevalence. *Bone* 2006; **38**: S4-S9.
- 6 Khosla S, Hofbauer LC. Osteoporosis treatment: recent developments and ongoing challenges. *Lancet Diabetes Endocrinol* 2017; **5**: 898-907.
- 7 Shane E, Burr D, Abrahamsen B, Adler RA, Brown TD, Cheung AM, et al. Atypical subtrochanteric and diaphyseal femoral fractures: second report of a task force of the American Society for Bone and Mineral Research. *J Bone Miner Res* 2014; **29**: 1-23.
- 8 Khosla S, Burr D, Cauley J, Dempster DW, Ebeling PR, Felsenberg D, et al. Bisphosphonate-associated osteonecrosis of the jaw: report of a task force of the American Society for Bone and Mineral Research. *J Bone Miner Res* 2007; **22**: 1479-91.
- 9 Reid IR, Miller PD, Brown JP, Kendler DL, Fahrleitner-Pammer A, Valter I, et al. Effects of denosumab on bone histomorphometry: the FREEDOM and STAND studies. *J Bone Miner Res* 2010; **25**: 2256-65.
- 10 Wang K, Chen Y, Gao S, Wang M, Ge M, Yang Q, et al. Norlichexanthone purified from plant endophyte prevents postmenopausal osteoporosis by targeting ER α to inhibit RANKL signaling. *Acta Pharm Sin B* 2021; **11**: 442-55.

- 11 Cummings SR, Ferrari S, Eastell R, Gilchrist N, Jensen JB, McClung M, et al. Vertebral fractures after discontinuation of denosumab: a *post hoc* analysis of the randomized placebo-controlled FREEDOM trial and its extension. *J Bone Miner Res* 2018; **33**: 190-8.
- 12 Khosla S, Hofbauer LC. Osteoporosis treatment: recent developments and ongoing challenges. *Lancet Diabetes Endocrinol* 2017; **5**: 898-907.
- 13 Rachner TD, Khosla S, Hofbauer LC. Osteoporosis: now and the future. *Lancet* 2011; **377**: 1276-87.
- 14 Chavassieux P, Chapurlat R, Portero-Muzy N, Roux JP, Garcia P, Brown JP, et al. Bone-forming and antiresorptive effects of romosozumab in postmenopausal women with osteoporosis: bone histomorphometry and microcomputed tomography analysis after 2 and 12 months of treatment. *J Bone Miner Res* 2019; **34**: 1597-608.
- 15 Saag KG, Petersen J, Brandi ML, Karaplis AC, Lorentzon M, Thomas T, et al. Romosozumab or alendronate for fracture prevention in women with osteoporosis. *N Engl J Med* 2017; **377**: 1417-27.
- 16 Ghaben AL, Scherer PE. Adipogenesis and metabolic health. *Nat Rev Mol Cell Biol* 2019; **20**: 242-58.
- 17 Yang X, Li J, Zhao L, Chen Y, Cui Z, Xu T, et al. Targeting adipocytic discoidin domain receptor 2 impedes fat gain while increasing bone mass. *Cell Death Differ* 2022; **29**: 737-49.
- 18 Cypess AM. Reassessing human adipose tissue. *N Engl J Med* 2022; **386**: 768-79.
- 19 Lumeng CN, Bodzin JL, Saltiel AR. Obesity induces a phenotypic switch in adipose tissue macrophage polarization. *J Clin Invest* 2007; **117**: 175-84.
- 20 Margaritis M, Antonopoulos AS, Digby J, Lee R, Reilly S, Coutinho P, et al. Interactions between vascular wall and perivascular adipose tissue reveal novel roles for adiponectin in the regulation of endothelial nitric oxide synthase function in human vessels. *Circulation* 2013; **127**: 2209-21.
- 21 Xie Z, Wang X, Liu X, Du H, Sun C, Shao X, et al. Adipose-derived exosomes exert proatherogenic effects by regulating macrophage foam cell formation and polarization. *J Am Heart Assoc* 2018; **7**: e007442.
- 22 Thomou T, Mori MA, Dreyfuss JM, Konishi M, Sakaguchi M, Wolfrum C, et al. Adipose-derived circulating miRNAs regulate gene expression in other tissues. *Nature* 2017; **542**: 450-5.
- 23 Lee YC, Chang HH, Chiang CL, Liu CH, Yeh JI, Chen MF, et al. Role of

perivascular adipose tissue-derived methyl palmitate in vascular tone regulation and pathogenesis of hypertension. *Circulation* 2011; **124**: 1160-71.

24 Rosen ED, Sarraf P, Troy AE, Bradwin G, Moore K, Milstone DS, et al. PPAR gamma is required for the differentiation of adipose tissue *in vivo* and *in vitro*. *Mol Cell* 1999; **4**: 611-7.

25 Gastaldelli A, Casolaro A, Ciociaro D, Frascerra S, Nannipieri M, Buzzigoli E, et al. Decreased whole body lipolysis as a mechanism of the lipid-lowering effect of pioglitazone in type 2 diabetic patients. *Am J Physiol Endocrinol Metab* 2009; **297**: E225-E30.

26 Prentice KJ, Saksi J, Robertson LT, Lee GY, Inouye KE, Eguchi K, et al. A hormone complex of FABP4 and nucleoside kinases regulates islet function. *Nature* 2021; **600**: 720-6.

27 Lodhi IJ, Yin L, Jensen-Urstad AP, Funai K, Coleman T, Baird JH, et al. Inhibiting adipose tissue lipogenesis reprograms thermogenesis and PPARgamma activation to decrease diet-induced obesity. *Cell Metab* 2012; **16**: 189-201.

28 Guilherme A, Pedersen DJ, Henchey E, Henriques FS, Danai LV, Shen Y, et al. Adipocyte lipid synthesis coupled to neuronal control of thermogenic programming. *Mol Metab* 2017; **6**: 781-96.

29 Lee KS, Lee J, Kim HK, Yeom SH, Woo CH, Jung YJ, et al. Extracellular vesicles from adipose tissue-derived stem cells alleviate osteoporosis through osteoprotegerin and miR-21-5p. *J Extracell Vesicles* 2021; **10**: e12152.

30 Dai B, Xu J, Li X, Huang L, Hopkins C, Wang H, et al. Macrophages in epididymal adipose tissue secrete osteopontin to regulate bone homeostasis. *Nat Commun* 2022; **13**: 427.

31 Liu P, Ji Y, Yuen T, Rendina-Ruedy E, DeMambro VE, Dhawan S, et al. Blocking FSH induces thermogenic adipose tissue and reduces body fat. *Nature* 2017; **546**: 107-12.

32 Zhu LL, Blair H, Cao J, Yuen T, Latif R, Guo L, et al. Blocking antibody to the β -subunit of FSH prevents bone loss by inhibiting bone resorption and stimulating bone synthesis. *Proc Natl Acad Sci U S A* 2012; **109**: 14574-9.

33 Zou W, Rohatgi N, Brestoff JR, Li Y, Barve RA, Tycksen E, et al. Ablation of fat cells in adult mice induces massive bone gain. *Cell Metab* 2020; **32**: 801-13.e6.

34 Ussar S, Wang H-V, Linder S, Fässler R, Moser M. The Kindlins: subcellular localization and expression during murine development. *Exp Cell Res* 2006; **312**: 3142-

51.

35 Shen Z, Ye Y, Dong L, Vainionpää S, Mustonen H, Puolakkainen P, et al. Kindlin-2: a novel adhesion protein related to tumor invasion, lymph node metastasis, and patient outcome in gastric cancer. *Am J Surg* 2012; **203**: 222-9.

36 Calderwood DA, Campbell ID, Critchley DR. Talins and kindlins: partners in integrin-mediated adhesion. *Nat Rev Mol Cell Biol* 2013; **14**: 503-17.

37 Sun Z, Costell M, Fässler R. Integrin activation by talin, kindlin and mechanical forces. *Nat Cell Biol* 2019; **21**: 25-31.

38 Li H, Deng Y, Sun K, Yang H, Liu J, Wang M, et al. Structural basis of kindlin-mediated integrin recognition and activation. *Proc Natl Acad Sci U S A* 2017; **114**: 9349-54.

39 Hirbawi J, Bialkowska K, Bledzka KM, Liu J, Fukuda K, Qin J, et al. The extreme C-terminal region of kindlin-2 is critical to its regulation of integrin activation. *J Biol Chem* 2017; **292**: 14258-69.

40 Gao H, Zhou L, Zhong Y, Ding Z, Lin S, Hou X, et al. Kindlin-2 haploinsufficiency protects against fatty liver by targeting Foxo1 in mice. *Nat Commun* 2022; **13**: 1025.

41 Yu J, Hu Y, Gao Y, Li Q, Zeng Z, Li Y, et al. Kindlin-2 regulates hepatic stellate cells activation and liver fibrogenesis. *Cell Death Discov* 2018; **4**: 34.

42 Qi L, Chi X, Zhang X, Feng X, Chu W, Zhang S, et al. Kindlin-2 suppresses transcription factor GATA4 through interaction with SUV39H1 to attenuate hypertrophy. *Cell Death Dis* 2019; **10**: 890.

43 Zhang Z, Mu Y, Zhang J, Zhou Y, Cattaneo P, Veevers J, et al. Kindlin-2 is essential for preserving integrity of the developing heart and preventing ventricular rupture. *Circulation* 2019; **139**: 1554-6.

44 Sun Y, Guo C, Ma P, Lai Y, Yang F, Cai J, et al. Kindlin-2 association with Rho GDP-dissociation inhibitor alpha suppresses Rac1 activation and podocyte injury. *J Am Soc Nephrol* 2017; **28**: 3545-62.

45 Zhu K, Lai Y, Cao H, Bai X, Liu C, Yan Q, et al. Kindlin-2 modulates MafA and β -catenin expression to regulate β -cell function and mass in mice. *Nat Commun* 2020; **11**: 484.

46 Cao H, Yan Q, Wang D, Lai Y, Zhou B, Zhang Q, et al. Focal adhesion protein Kindlin-2 regulates bone homeostasis in mice. *Bone Res* 2020; **8**: 2.

47 Wu C, Jiao H, Lai Y, Zheng W, Chen K, Qu H, et al. Kindlin-2 controls TGF-beta signalling and Sox9 expression to regulate chondrogenesis. *Nat Commun* 2015; **6**: 7531.

- 48 Fu X, Zhou B, Yan Q, Tao C, Qin L, Wu X, et al. Kindlin-2 regulates skeletal homeostasis by modulating PTH1R in mice. *Signal Transduct Target Ther* 2020; **5**: 297.
- 49 Chen S, He T, Zhong Y, Chen M, Yao Q, Chen D, et al. Roles of focal adhesion proteins in skeleton and diseases. *Acta Pharm Sin B* 2023; **13**: 998-1013.
- 50 Lee KY, Russell SJ, Ussar S, Boucher J, Vernochet C, Mori MA, et al. Lessons on conditional gene targeting in mouse adipose tissue. *Diabetes* 2013; **62**: 864-74.
- 51 Gao H, Guo Y, Yan Q, Yang W, Li R, Lin S, et al. Lipoatrophy and metabolic disturbance in mice with adipose-specific deletion of kindlin-2. *JCI Insight* 2019; **4**: e128405.
- 52 Lei Y, Fu X, Li P, Lin S, Yan Q, Lai Y, et al. LIM domain proteins Pinch1/2 regulate chondrogenesis and bone mass in mice. *Bone Res* 2020; **8**: 37.
- 53 Wang Y, Yan Q, Zhao Y, Liu X, Lin S, Zhang P, et al. Focal adhesion proteins Pinch1 and Pinch2 regulate bone homeostasis in mice. *JCI Insight* 2019; **4**: e131692.
- 54 Cao H, Yu S, Yao Z, Galson DL, Jiang Y, Zhang X, et al. Activating transcription factor 4 regulates osteoclast differentiation in mice. *J Clin Invest* 2010; **120**: 2755-66.
- 55 Cao H, Zhu K, Qiu L, Li S, Niu H, Hao M, et al. Critical role of AKT protein in myeloma-induced osteoclast formation and osteolysis. *J Biol Chem* 2013; **288**: 30399-410.
- 56 Gao H, Zhong Y, Ding Z, Lin S, Hou X, Tang W, et al. Pinch loss ameliorates obesity, glucose intolerance, and fatty liver by modulating adipocyte apoptosis in mice. *Diabetes* 2021; **70**: 2492-505.
- 57 Yan Q, Gao H, Yao Q, Ling K, Xiao G. Loss of phosphatidylinositol-4-phosphate 5-kinase type-1 gamma (*Pip5k1c*) in mesenchymal stem cells leads to osteopenia by impairing bone remodeling. *J Biol Chem* 2022; **298**: 101639.
- 58 Qin TT, Xu GC, Qi JW, Yang GL, Zhang K, Liu HL, et al. Tumour necrosis factor superfamily member 15 (*Tnfsf15*) facilitates lymphangiogenesis via up-regulation of *Vegfr3* gene expression in lymphatic endothelial cells. *J Pathol* 2015; **237**: 307-18.
- 59 Konermann S, Lotfy P, Brideau NJ, Oki J, Shokhirev MN, Hsu PD. Transcriptome engineering with RNA-targeting Type VI-D CRISPR effectors. *Cell* 2018; **173**: 665-76.e14.
- 60 Huang W, Liu X, Queen NJ, Cao L. Targeting visceral fat by intraperitoneal delivery of novel AAV serotype vector restricting off-target transduction in liver. *Mol Ther Methods Clin Dev* 2017; **6**: 68-78.
- 61 Cummings SR, San Martin J, McClung MR, Siris ES, Eastell R, Reid IR, et al.

- Denosumab for prevention of fractures in postmenopausal women with osteoporosis. *N Engl J Med* 2009; **361**: 756-65.
- 62 Brotto M, Bonewald L. Bone and muscle: interactions beyond mechanical. *Bone* 2015; **80**: 109-14.
- 63 Tagliaferri C, Wittrant Y, Davicco MJ, Walrand S, Coxam V. Muscle and bone, two interconnected tissues. *Ageing Res Rev* 2015; **21**: 55-70.
- 64 Tontonoz P, Graves RA, Budavari AI, Erdjument-Bromage H, Lui M, Hu E, et al. Adipocyte-specific transcription factor ARF6 is a heterodimeric complex of two nuclear hormone receptors, PPAR gamma and RXR alpha. *Nucleic Acids Res* 1994; **22**: 5628-34.
- 65 Garin-Shkolnik T, Rudich A, Hotamisligil GS, Rubinstein M. FABP4 attenuates PPAR γ and adipogenesis and is inversely correlated with PPAR γ in adipose tissues. *Diabetes* 2014; **63**: 900-11.
- 66 Wei W, Wang X, Yang M, Smith LC, Dechow PC, Sonoda J, et al. PGC1beta mediates PPARgamma activation of osteoclastogenesis and rosiglitazone-induced bone loss. *Cell Metab* 2010; **11**: 503-16.
- 67 Zhang S, Yu M, Guo F, Yang X, Chen Y, Ma C, et al. Rosiglitazone alleviates intrahepatic cholestasis induced by α -naphthylisothiocyanate in mice: the role of circulating 15-deoxy- Δ (12,14)-PGJ(2) and Nogo. *Br J Pharmacol* 2020; **177**: 1041-60.
- 68 Fulzele K, Riddle RC, DiGirolamo DJ, Cao X, Wan C, Chen D, et al. Insulin receptor signaling in osteoblasts regulates postnatal bone acquisition and body composition. *Cell* 2010; **142**: 309-19.
- 69 DeMambro VE, Kawai M, Clemens TL, Fulzele K, Maynard JA, Marín de Evsikova C, et al. A novel spontaneous mutation of *Irs1* in mice results in hyperinsulinemia, reduced growth, low bone mass and impaired adipogenesis. *J Endocrinol* 2010; **204**: 241-53.
- 70 Xi G, Shen X, Rosen CJ, Clemmons DR. IRS-1 functions as a molecular scaffold to coordinate IGF-I/IGFBP-2 signaling during osteoblast differentiation. *J Bone Miner Res* 2016; **31**: 1300-14.
- 71 Yamaguchi M, Ogata N, Shinoda Y, Akune T, Kamekura S, Terauchi Y, et al. Insulin receptor substrate-1 is required for bone anabolic function of parathyroid hormone in mice. *Endocrinology* 2005; **146**: 2620-8.
- 72 Malekzadeh B, Tengvall P, Ohrnell LO, Wennerberg A, Westerlund A. Effects of locally administered insulin on bone formation in non-diabetic rats. *J Biomed Mater*

Res A 2013; **101**: 132-7.

73 Thrailkill K, Bunn RC, Lumpkin C Jr, Wahl E, Cockrell G, Morris L, et al. Loss of insulin receptor in osteoprogenitor cells impairs structural strength of bone. *J Diabetes Res* 2014; **2014**: 703589.

74 Barrett-Connor E, Kritiz-Silverstein D. Does hyperinsulinemia preserve bone?. *Diabetes Care* 1996; **19**: 1388-92.

75 Jones SF, Infante JR. Molecular pathways: fatty acid synthase. *Clin Cancer Res* 2015; **21**: 5434-8.

76 Lodhi IJ, Yin L, Jensen-Urstad AP, Funai K, Coleman T, Baird JH, et al. Inhibiting adipose tissue lipogenesis reprograms thermogenesis and PPAR γ activation to decrease diet-induced obesity. *Cell Metab* 2012; **16**: 189-201.

77 Liu J, Wang Y, Lin L. Small molecules for fat combustion: targeting obesity. *Acta Pharm Sin B* 2019; **9**: 220-36.

78 Blanquart C, Barbier O, Fruchart JC, Staels B, Glineur C. Peroxisome proliferator-activated receptors: regulation of transcriptional activities and roles in inflammation. *J Steroid Biochem Mol Biol* 2003; **85**: 267-73.

79 Cristancho AG, Lazar MA. Forming functional fat: a growing understanding of adipocyte differentiation. *Nat Rev Mol Cell Biol* 2011; **12**: 722-34.

80 Wakabayashi K, Okamura M, Tsutsumi S, Nishikawa NS, Tanaka T, Sakakibara I, et al. The peroxisome proliferator-activated receptor gamma/retinoid X receptor alpha heterodimer targets the histone modification enzyme PR-Set7/Setd8 gene and regulates adipogenesis through a positive feedback loop. *Mol Cell Biol* 2009; **29**: 3544-55.

81 Weber DR, Haynes K, Leonard MB, Willi SM, Denburg MR. Type 1 diabetes is associated with an increased risk of fracture across the life span: a population-based cohort study using The Health Improvement Network (THIN). *Diabetes Care* 2015; **38**: 1913-20.

82 Ferron M, Wei J, Yoshizawa T, Del Fattore A, DePinho RA, Teti A, et al. Insulin signaling in osteoblasts integrates bone remodeling and energy metabolism. *Cell* 2010; **142**: 296-308.

83 Kim YC, Lee SE, Kim SK, Jang HD, Hwang I, Jin S, et al. Toll-like receptor mediated inflammation requires FASN-dependent MYD88 palmitoylation. *Nat Chem Biol* 2019; **15**: 907-16.

84 Loomba R, Mohseni R, Lucas KJ, Gutierrez JA, Perry RG, Trotter JF, et al. TVB-2640 (FASN inhibitor) for the treatment of nonalcoholic steatohepatitis: FASCINATE-

1, a randomized, placebo-controlled phase 2a trial. *Gastroenterology* 2021; **161**: 1475-86.

85 Fhu CW, Ali A. Fatty acid synthase: an emerging target in cancer. *Molecules* 2020; **25**: 3935.

Journal Pre-proof

Figure captions

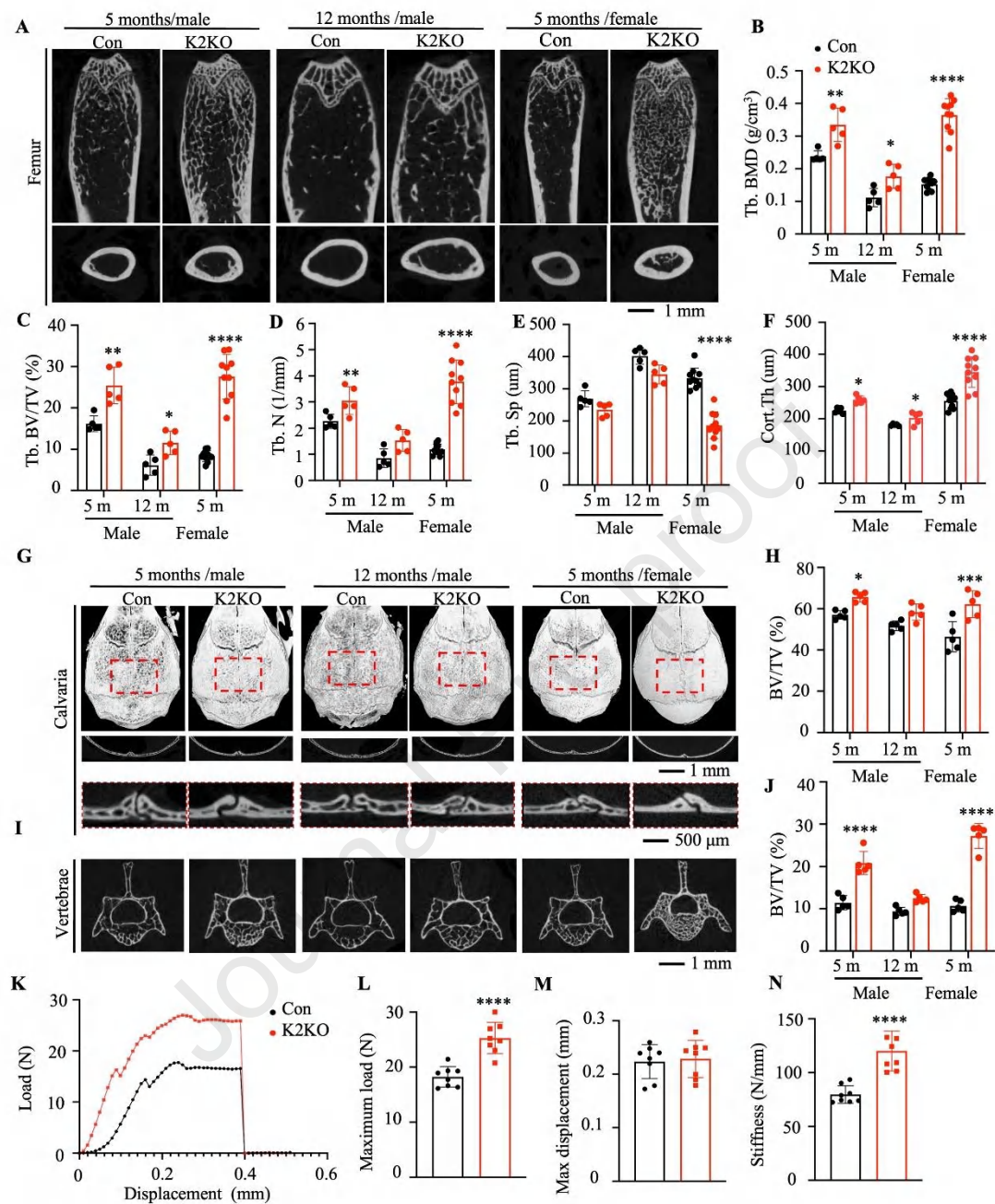


Figure 1 Adipocyte-targeted deletion of Kindlin-2 dramatically increases bone mass. (A) Three-dimensional (3D) reconstruction from μ CT scans of the distal femurs of K2KO mice and Con mice with the indicated sexes and ages. Scale bar, 1 mm. (B)–(F) Quantitative analyses of BMD, BV/TV, Tb.N, Tb.Sp and Cort.Th of distal femurs of K2KO mice and Con mice with the indicated sexes and ages. $n = 10$, 5-month-old female K2KO mice; $n = 5$ mice in the remaining groups. (G) 3D reconstruction from μ CT scans of the whole calvaria from control and K2KO mice (top figures). Scale bar,

1 mm. μ CT cross-section view of the suture of parietal and interparietal bones (middle figures). Scale bar, 1 mm. μ CT analysis of the ROI of $2 \times 2 \text{ mm}^2$ area in the center of the parietal bone (bottom figures), which is highlighted in red square. Scale bar, 500 μm . (H) Quantitative analyses of BV/TV of μ CT data of calvaria ROI in K2KO and control mice. $n = 5$ for each group. (I) μ CT scans of L4 spinal vertebral body bone. Scale bar, 1 mm. (J) Quantitative analyses of BV/TV of μ CT data of vertebral body bone. $n = 5$ for each group. $*P < 0.05$, $**P < 0.01$, $***P < 0.001$, $****P < 0.0001$, *versus* controls. One-way ANOVA, followed by Tukey multiple comparisons post test. (K) Representative force-displacement curve for femurs from control and K2KO mice. (L)–(N) Quantification data of maximum load, maximum displacement, and stiffness for the femurs from control and K2KO mice. $n = 8$ for each group. Bone samples were from 5-month-old female mice. $*P < 0.05$, $**P < 0.01$, $***P < 0.001$, $****P < 0.0001$, *versus* controls. Student's t test. Results are expressed as the mean \pm standard deviation (SD).

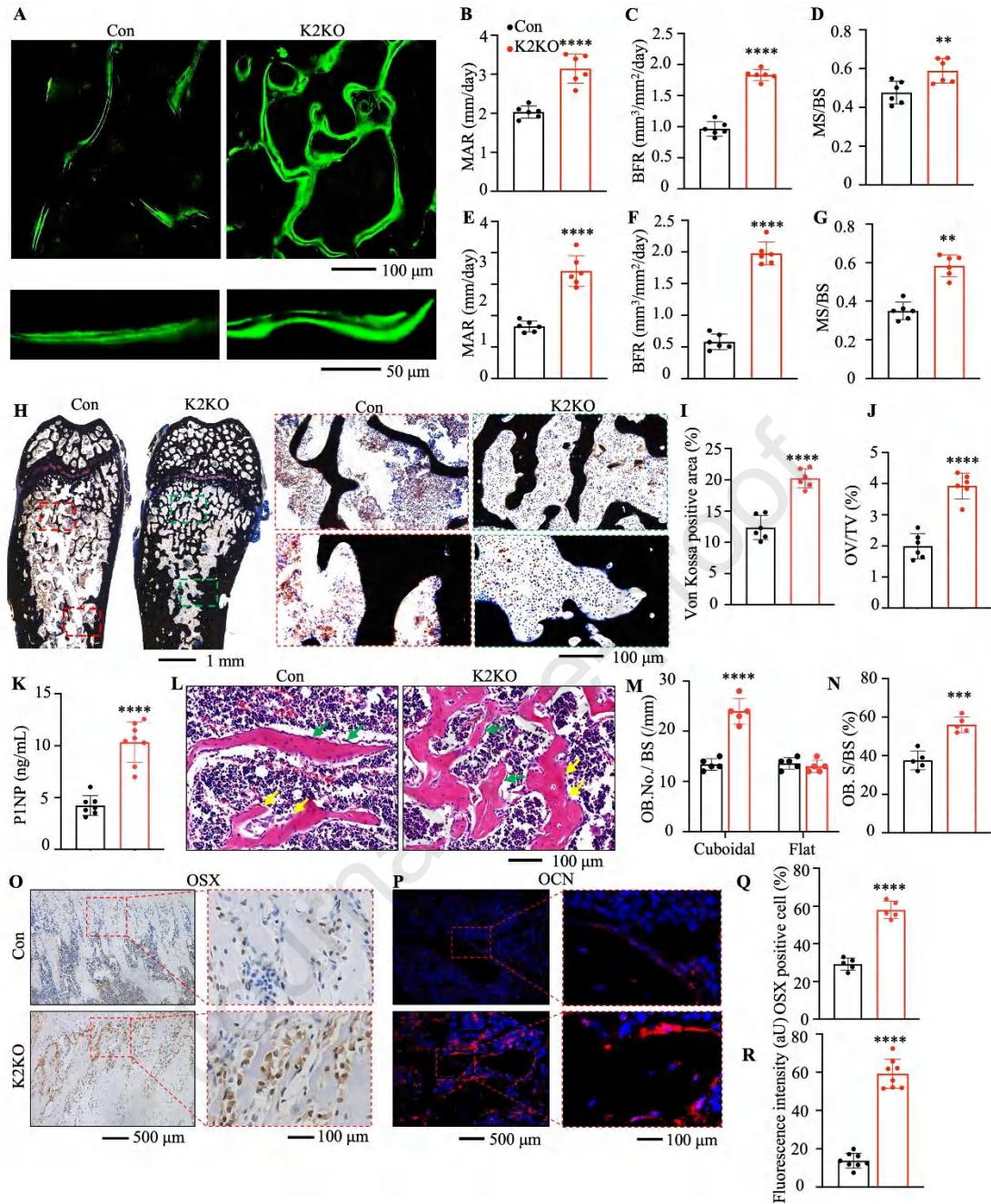


Figure 2 Kindlin-2 loss strikingly increases osteoblast differentiation and bone formation *in vivo*. (A)–(G) Calcein double labeling experiment. Representative images of femoral sections from 5-month-old K2KO and control mice (A). Scale bar, 100 μ m and 50 μ m. Sections of nondemineralized femurs of 5-month-old K2KO and control mice were used for measurements of MAR (B, E), bone formation rate (BFR) (C, F) and MS/BS (D, G) for metaphyseal trabecular bones (A, top figures) and cortical bones (A, bottom figures). $n = 6$ in each group. (H)–(J) Von Kossa staining of

nondemineralized femoral sections. Representative images of femoral sections from 5-month-old K2KO and control mice (H). Scale bar, 1 mm and 100 μm . Quantification of von Kossa positive area (I) and osteoid volume/total volume (OV/TV). $n = 6$ in each group. (K) ELISA assay of serum level of procollagen type 1 amino-terminal propeptide (P1NP). Sera from 5-month-old control and K2KO mice were used for ELISA assay for P1NP. $n = 7$ mice in control group, $n = 8$ mice in K2KO group. (L) Representative images of H&E staining of femur trabecular bones of 5-month-old K2KO and control littermates. Yellow arrows indicate cuboidal osteoblasts and green arrows indicate flat osteoblasts. Quantification of OB. No./BS (M) and OB. S/BS (N). $n = 5$ mice for each group. Scale bar, 100 μm . (O) IHC staining of OSX. Tibial sections from 5-month-old control and K2KO mice were subjected to IHC staining for OSX expression. Scale bar, 500 μm , 100 μm . (Q) Quantification analysis of (O). $n = 5$ mice per group. (P) IF staining of OCN. Tibial sections from 5-month-old control and K2KO mice were subjected to IF staining for OCN expression. Scale bar, 500 μm , 100 μm . (R) Quantification analysis of (P). $n = 8$ mice per group. $*P < 0.05$, $**P < 0.01$, $***P < 0.001$, $****P < 0.0001$ versus controls. Student's t test. Results are expressed as mean \pm SD.

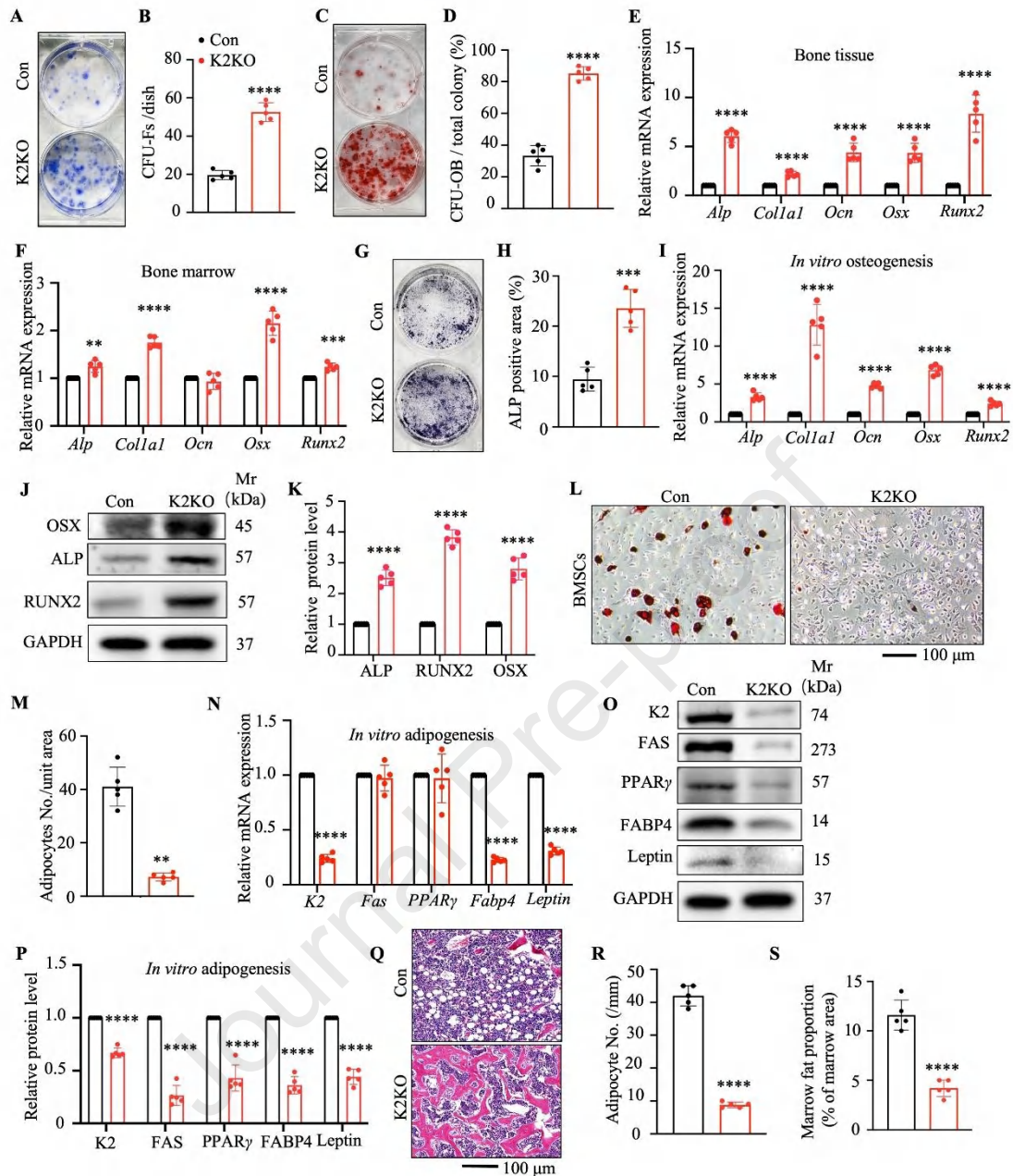


Figure 3 Kindlin-2 loss increases osteogenic while decreases adipogenic differentiation of BMSCs. (A) CFU-F assays determined by Giemsa staining. (B) The number of CFU-F was scored under a microscope. $n = 5$ mice per group. (C) CFU-OB assays. (D) The number of CFU-OB was scored under a microscope. $n = 5$ mice per group. (E) RT-qPCR analyses using RNA samples isolated from fresh bone tissues. **** $P < 0.0001$, versus controls, Student's t test. $n = 5$ mice per group. (F) RT-qPCR analyses using RNA samples isolated from fresh bone marrows. $n = 5$ mice per group. (G) ALP staining. (H) Quantification analysis of (G). *** $P < 0.001$, versus controls, Student's t test. $n = 5$ mice per genotype. The results are expressed as the mean \pm SD. (I) RT-qPCR analyses.

RNA samples were isolated from primary BMSCs after being induced for osteoblastic differentiation for 7 days *in vitro*. $n = 5$ mice per group. (J, K) WB analyses. Protein extracts were isolated from primary BMSCs after being induced for osteoblastic differentiation for 7 days *in vitro*. $n = 5$ mice per group. (L, M) *In vitro* adipogenic differentiation. Primary BMSCs isolated from 5-month-old control and K2KO mice were cultured with adipogenic medium for 7 days, followed by oil red O staining (L), RT-qPCR analyses (N) and WB analyses (O, P). Quantitative data for L (M) and O (P). $n = 5$ biologically independent experiments. (Q) H&E staining. 5 μm tibiae sections of 5-month-old control and K2KO male mice were subjected to H&E staining. Adipocyte number (R) and marrow fat proportion (S) were calculated. $n = 5$ mice in each group. $*P < 0.05$, $**P < 0.01$, $***P < 0.001$, $****P < 0.0001$ versus controls, Student's *t* test.

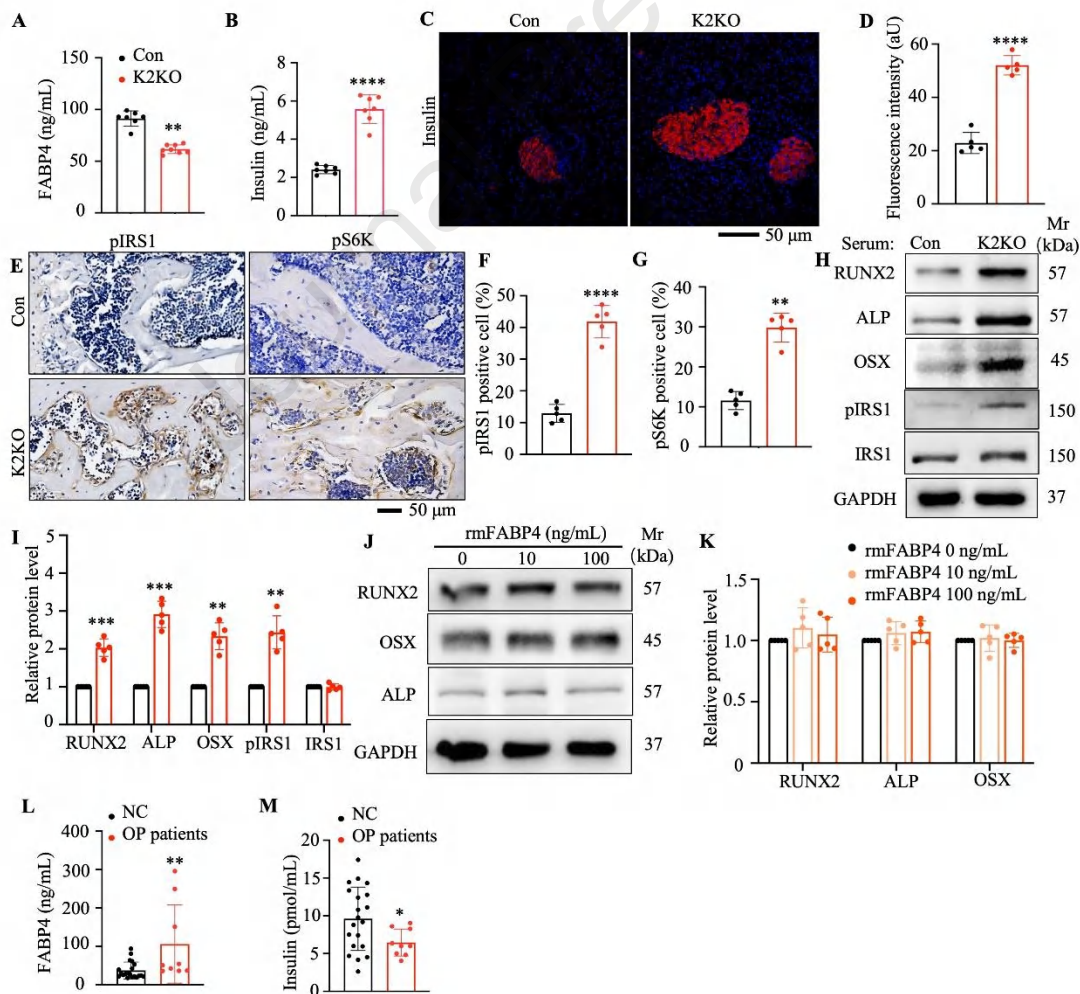


Figure 4 KINDLIN-2 loss decreases FABP4 and increases insulin expression. (A, B)

ELISA assay of serum level of FABP4 and insulin. Sera from 5-month-old control and K2KO mice were used for ELISA assay for FABP4 and insulin. $n = 7$ mice in each group. (C) IF staining of insulin. Pancreatic sections from 5-month-old control and K2KO mice were subjected to IF staining for insulin expression. Scale bar, 50 μm . (D) Quantification analysis of (C). $n = 5$ mice per group. (E) IHC staining of pIRS1 and pS6K. Tibial sections from 5-month-old control and K2KO mice were subjected to IHC staining of pIRS1 and pS6K. Scale bar, 50 μm . (F, G) Quantification analysis of (E). $n = 5$ mice per group. (H, I) WB analyses. Protein extracts were isolated from primary BMSCs after being treated with serum obtained from control and K2KO mice. Serum was from 5 mice per genotype. $n = 5$ biologically independent experiments. (J, K) WB analyses. Protein extracts were isolated from primary BMSCs after being treated with different doses of rmFABP4. $n = 5$ biologically independent experiments. (L) Serum level of FABP4 was increased in OP patients revealed by ELISA assay. (M) Serum level of insulin was decreased in OP patients revealed by ELISA assay. $n = 20$ for NC group, $n = 9$ for OP group. $*P < 0.05$, $**P < 0.01$, $***P < 0.001$, $****P < 0.0001$ versus controls. Student's t test. Results are expressed as mean \pm SD.

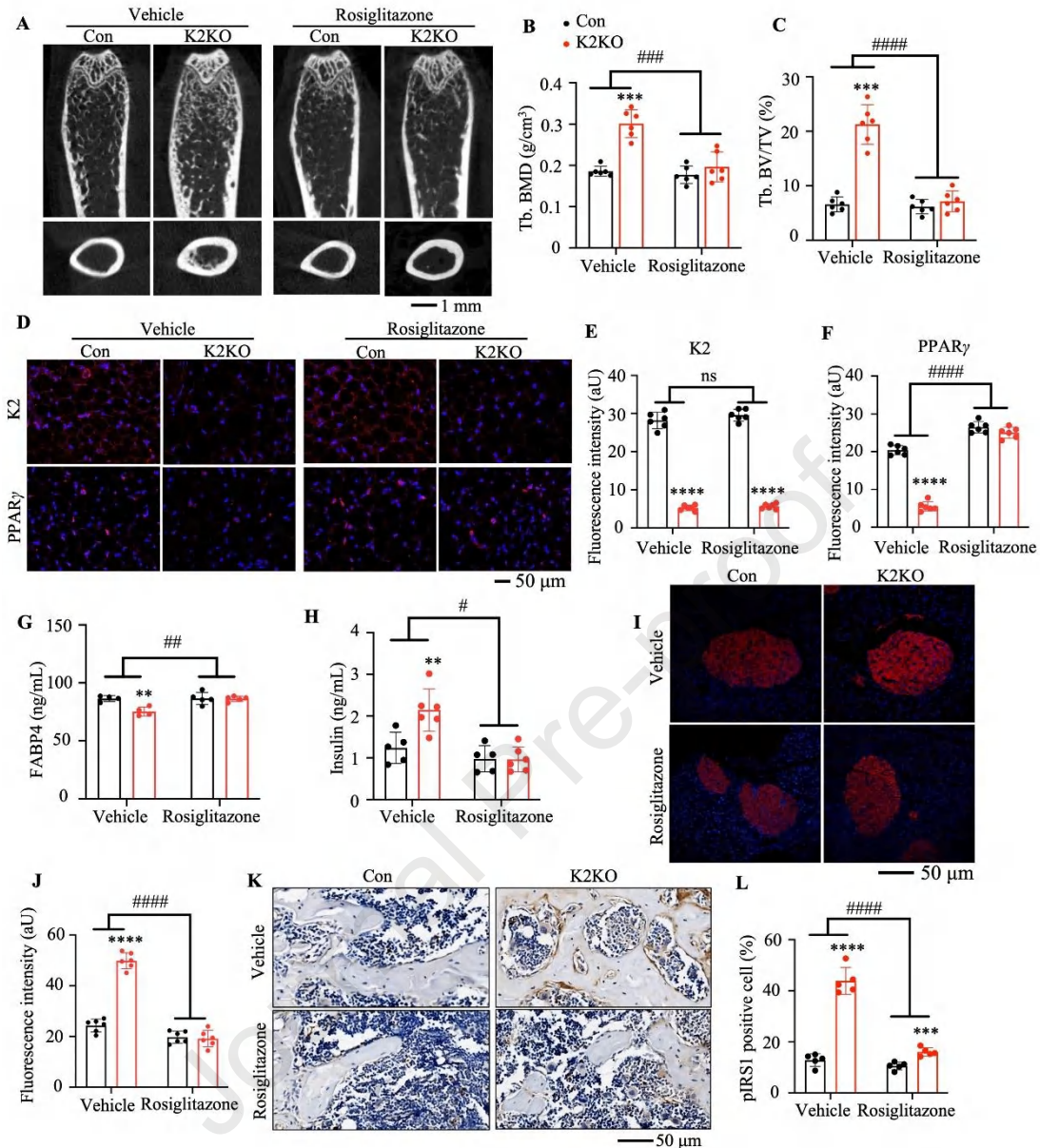


Figure 5 Rosiglitazone treatment reverses the high bone mass phenotype of K2KO mice. 3-month-old K2KO and control mice were treated with rosiglitazone (30 mg/kg/day) or vehicle (1% carboxymethylcellulose in saline) daily, by oral gavage for 1 month, then samples were collected for the following assays. (A) 3D reconstruction from μ CT scans of the distal femurs. Scale bar, 1 mm. Quantitative analyses of BMD (B) and BV/TV (C). $n = 6$ mice in each group. (D)–(F) IF staining of Kindlin-2 and PPAR γ . (G, H) ELISA assay of serum level of FABP4 and insulin. $n = 4$ –6 mice per group. (I) IF staining of insulin. Scale bar, 50 μ m. (J) Quantification analysis of (I). $n = 6$ mice per group. (K) IHC staining of pIRS1. Tibial sections were subjected to IHC

staining of pIRS1. Scale bar, 50 μ m. (L) Quantification analysis of (K). $n = 5$ mice per group. * $P < 0.05$, ** $P < 0.01$, *** $P < 0.001$, **** $P < 0.0001$ versus controls. Student's t test. # $P < 0.05$, ## $P < 0.01$, ### $P < 0.001$, #### $P < 0.0001$ versus controls. Two-way ANOVA. Results are expressed as the mean \pm SD.

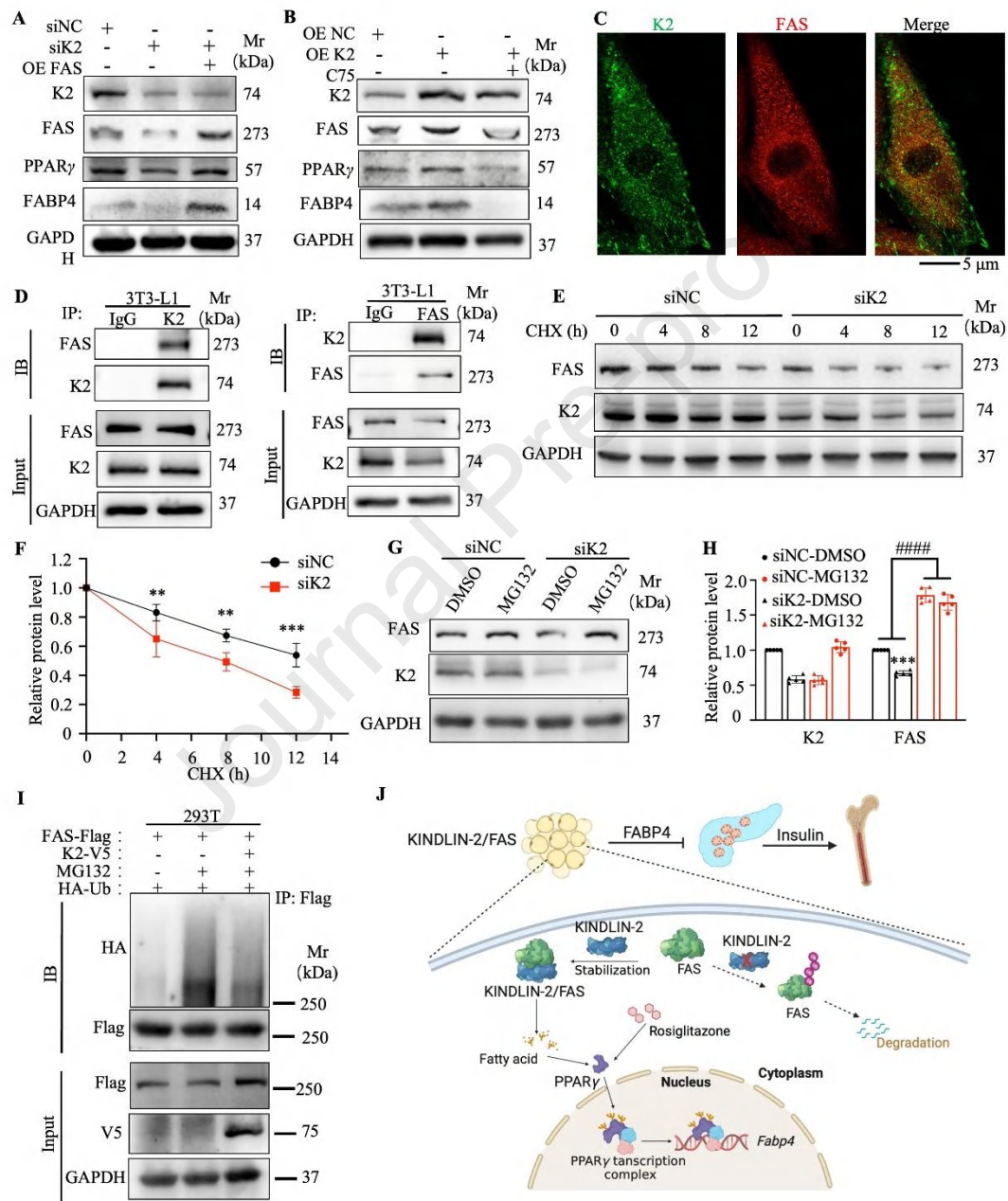


Figure 6 Kindlin-2 controls PPAR γ and FABP4 expression through modulating proteasome-mediated FAS degradation. (A) FAS overexpression blocks the decrease of PPAR γ and FABP4 caused by KINDLIN-2 knockdown. siRNA for Kindlin-2 (siK2) or

negative control (siNC) and plasmid expressing FAS (OE FAS) were used to transfect 3T3-L1 preadipocyte, followed by WB. (B) FAS inhibitor C75 blocks the increase of PPAR γ and FABP4 caused by Kindlin-2 overexpression. Plasmid expressing K2 (OE K2) or negative control (OE NC) were used to transfect 3T3-L1 preadipocyte, followed by WB. (C) IF staining. 3T3-L1 preadipocytes were used for double immunostaining of KINDLIN-2 (green) and FAS (red), then visualized with confocal microscopy. Scale bar, 5 μ m. (D) Co-IP assays. Cell lysates from 3T3-L1 preadipocytes were used for IP and IB assays with the indicated antibodies for the detection of the endogenous interaction between Kindlin-2 and FAS. (E, F) Cycloheximide (CHX) experiments. HEK293T cells with and without siK2 were treated with CHX (100 μ g/mL) for the indicated times, followed by WB analyses. $n = 3$ biologically independent experiments. $*P < 0.05$, $**P < 0.01$, $***P < 0.001$. One-way ANOVA, followed by Tukey multiple comparisons posttest. (G, H) MG132 treatment experiment. HEK293T cells with and without siK2 were treated with MG132 (10 μ mol/L) for 6 h, followed by WB. $n = 3$ biologically independent experiments. $*P < 0.05$, $**P < 0.01$, $***P < 0.001$, $****P < 0.0001$ versus control. Student's t test. $^{\#}P < 0.05$, $^{\#\#}P < 0.01$, $^{\#\#\#}P < 0.001$, $^{\#\#\#\#}P < 0.0001$ versus controls. Two-way ANOVA. Results are expressed mean \pm SD. (I) FAS ubiquitination. HEK293T cells were transfected with the indicated plasmids. 48 h after transfection, the cells were treated with MG132 (10 μ mol/L) for 6 h, followed by IB assays. (J) Working model of this study. For IP assays, 200 μ g of whole-cell extracts from each group were used. Immunoprecipitates were resuspended in 50 μ L buffer. 15 μ L from each sample was loaded for SDS-PAGE, followed by IB assays. Protein extracts (20 μ g) were used for WB analyses from each input sample for (bottom input panels). Data are representative of 5 biologically independent replicates.

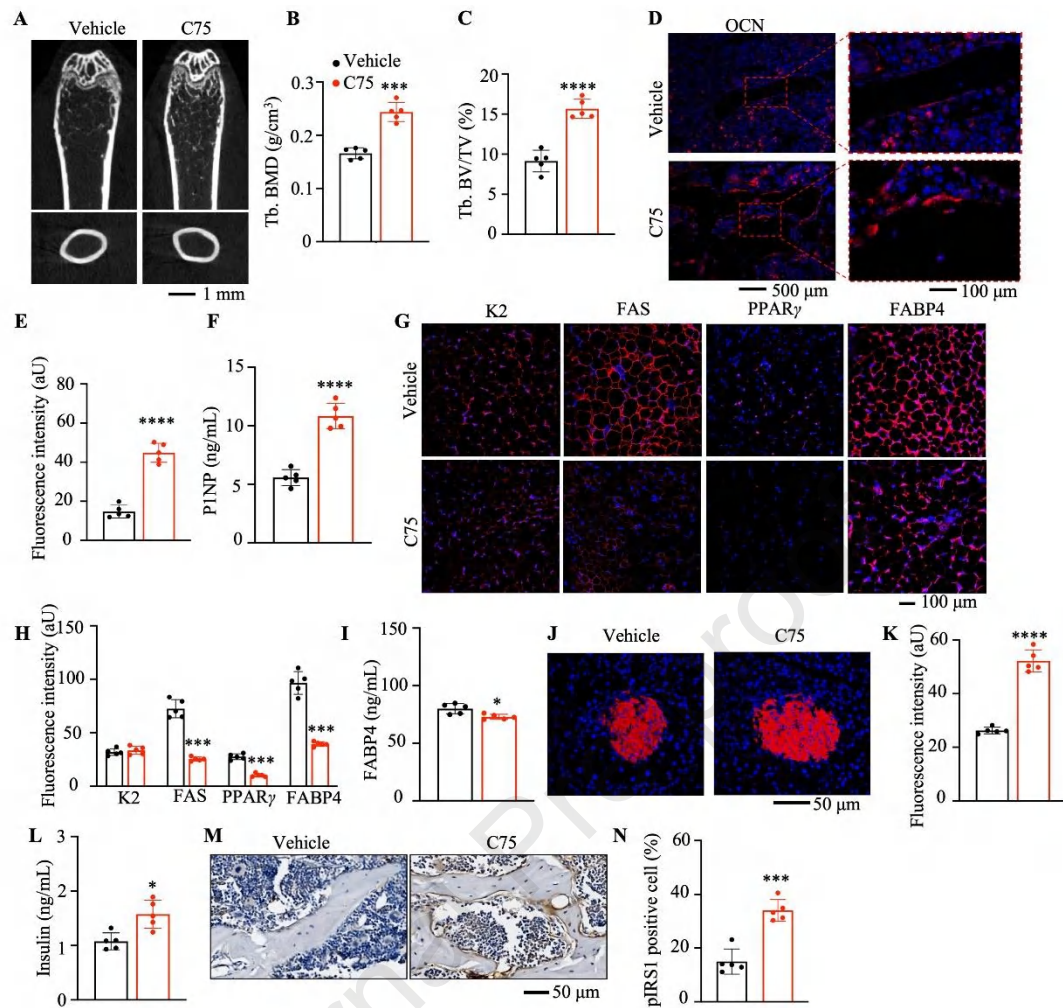


Figure 7 FAS inhibitor C75 treatment increases bone mass of C57BL/6 mice. 3-Month-old WT C57BL/6 mice were intraperitoneally injected with FAS inhibitor C75 (10 mg/kg) or vehicle (corn oil) every 72 h for 1 month, then samples were collected for the following assays. (A) 3D reconstruction from μ CT scans of the distal femurs. Scale bar, 1 mm. Quantitative analyses of BMD (B) and BV/TV (C). (D)–(E) IF staining of OCN. (F) ELISA assay of serum level of P1NP. (G, H) IF staining of KINDLIN-2, FAS, PPAR γ , and FABP4 in eWAT. (I) ELISA assay of serum level of FABP4. (J, K) IF staining of insulin expression. Scale bar, 50 μ m. (L) ELISA assay of serum level of insulin. (M, N) IHC staining of pIRS1. Tibial sections were subjected to IHC staining of pIRS1. Scale bar, 50 μ m. $n = 5$ mice for each group. * $P < 0.05$, ** $P < 0.01$, *** $P < 0.001$, **** $P < 0.0001$ versus controls. Student's t test. Results are expressed as the mean \pm SD.

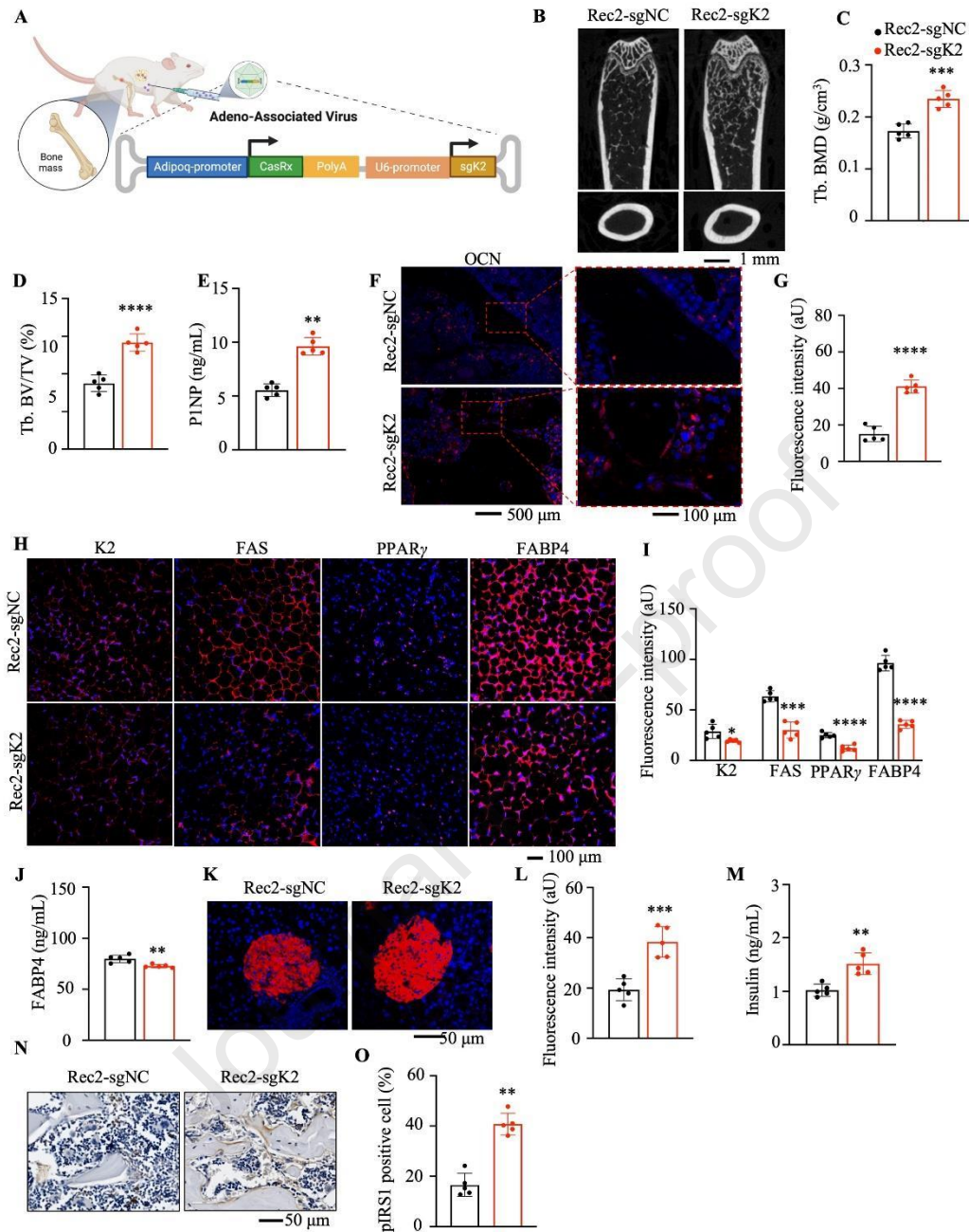


Figure 8 AAV-CasRx mediated RNA editing of Kindlin-2 in adipocytes increases bone mass of C57BL/6 mice. 3-Month-old WT C57BL/6 mice were intraperitoneally injected with AAV-Rec2-CasRx-sgK2 (Rec2-sgK2) or AAV-Rec2-CasRx-sgNC (Rec2-sgNC), 2 months later, samples were harvested for the following assays. (A) Diagram depicting the construction of the specific AAV. (B) 3D reconstruction from μ CT scans of the distal femurs. Scale bar, 1 mm. Quantitative analyses of BMD (C) and BV/TV (D). (E) ELISA assay of serum level of P1NP. (F, G) IF staining of OCN. (H, I) IF

staining of KINDLIN-2, FAS, PPAR γ , and FABP4 in eWAT. (J) ELISA assay of serum level of FABP4. (K, L) IF staining of insulin expression. Scale bar, 50 μ m. (M) ELISA assay of serum level of insulin. (N, O) IHC staining of pIRS1. Tibial sections were subjected to IHC staining of pIRS1. Scale bar, 50 μ m. $n = 5$ mice for each group. $*P < 0.05$, $**P < 0.01$, $***P < 0.001$, $****P < 0.0001$ versus controls. Student's t test. Results are expressed as the mean \pm SD

Journal Pre-proof

